ulm university universität ulm

Substitution of T403R allows efficient utilization of human ACE2 by Spike proteins of bat coronaviruses

Dissertation submitted in partial fulfillment of the requirements for the degree of Doctor rerum naturalium (Dr. rer. nat.) of the Faculty of Natural Sciences.

Institute of Molecular Virology Ulm University
Head: Prof. Dr. Frank Kirchhoff

Author: Fabian Daniel Zech

Born in Erlangen (Germany)

2022

Current dean of the Faculty:	Prof. Dr. Thorsten Bernhardt
1st supervisor:	Prof. Dr. Frank Kirchhoff
2nd supervisor:	Prof. Dr. Timo Jacob
Day doctorate awarded:	January 10, 2023

Results gained in my thesis have previously been published in the following publications:

“Spike residue 403 affects binding of coronavirus spikes to human ACE2”
Fabian Zech, Daniel Schniertshauer, Christoph Jung, Alexandra Herrmann, Arne Cordsmeier, Qinya Xie, Rayhane Nchioua, Caterina Prelli Bozzo, Meta Volcic, Lennart Koepke, Janis A. Müller, Jana Krüger, Sandra Heller, Steffen Stenger, Markus Hoffmann, Stefan Pöhlmann, Alexander Kleger, Timo Jacob, Karl-Klaus Conzelmann, Armin Ensser, Konstantin M.J. Sparrer and Frank Kirchhoff; doi: 10.1038/s41467-021-27180-0, Nature Communications; 2021

“Severe Acute Respiratory Syndrome Coronavirus 2 Vaccination boosts Neutralizing Activity against Seasonal Human Coronaviruses”
Jan Lawrenz, Qinya Xie, Fabian Zech, Tatjana Weil, Alina Seidel, Daniela Krnavek, Lia van der Hoek, Jan Münch, Janis A. Müller, and Frank Kirchhoff; doi: 10.1093/cid/ciac057, Clin Infect Dis; 2022

Table of contents

List of abbreviations vii

Bases ix

One letter amino acid code: ix

1. INTRODUCTION 1

1.1 COVID-19, a new zoonotic disease 1

1.2 SARS-CoV-2 emerged from bats in Southeast Asia 3

1.2.1 The versatile CoV Spike proteins 4

1.2.2 Structure of the CoV Spike and initial human adaptions 4

1.2.3 The Spike protein, a target for drugs and a template for vaccines 5

1.3 Scope of the study 7

2. MATERIALS & METHODS 8

2.1 Materials 8

2.1.1 Eukaryotic cells 8

2.1.2 Primary cells and tissue 9

2.1.3 Bacteria 9

2.1.4 Viruses 9

2.1.5 Nucleic acids 9

2.1.6 Primers 10

2.1.7 Antibodies 10

2.1.8 Enzymes 11

2.1.9 Buffers 11

2.1.10 Media 12

2.1.11 Reagents 13

2.1.12 Consumables 15

2.1.13 Kits 15

2.1.14 Technical equipment 16

2.1.15 Software 17
2.1.16 Other External facilities 17
2.2 Methods 18
2.2.1 Plasmid DNA preparation 18
2.2.2 Restriction Digest 18
2.2.3 Agarose gel electrophoresis 18
2.2.4 Transformation of bacteria 18
2.2.5 Culture of bacteria 18
2.2.6 Cell culture 19
2.2.7 Viruses and viral particles 19
2.2.8 Transfections 20
2.2.9 Molecular dynamics simulation 20
2.2.10 Whole-cell and cell-free lysates 20
2.2.11 SDS-PAGE and immunoblotting 21
2.2.12 ACE2 interaction assay 21
2.2.13 Stem Cell Culture and Intestinal Differentiation 22
2.2.14 Intestinal organoids 22
2.2.15 Sera from vaccinated individuals and ethics approval 23
2.2.16 Treatment with ATN-161 23
2.2.17 Sequence logo and alignments. 23
2.2.18 Statistics 24
3. RESULTS 25
3.1 RaTG13 S pp poorly infect SARS-CoV-2 permissive Caco-2 cells 25
3.2 SARS-COV-2 S R403 contributes to ACE2 binding 25
3.3 T403R allows RaTG13 Spike to use human ACE2 as receptor 27
3.4 The enhancing effect of T403R depends on E37 in ACE2. 29
3.5 RaTG13 S T403R increases ACE2-dependent proteolytic processing. 31

3.6 The ability of T403R RaTG13 S to utilize ACE2 is species-specific. 34

3.7 COVID-19 vaccination cross-neutralizes SARS-CoV-1 spike and enhances inhibition of hCoV-OC43 spike mediated infection..... 35

3.8 RaTG13 S T403R is sensitive to sera from vaccinated individuals. 36

4. Discussion..... 38

5. Summary..... 43

6. Appendix lvi

7. Aknowledgements lviii

8. Statutory declaration..... lix

List of abbreviations

+	Positive
°C	degree(s) Celsius
µ	micro (10^{-6})
µl	microliter
µM	Micromolar
3’	3 prime
5’	5 prime
A	Ampere
Ab	Antibody
ATCC	American Type Culture Collection
Amp	Ampicillin
BSA	bovine serum albumin
bp	Base pair
$CaCl_2$	Calcium Chloride
CO2	Carbon Dioxide
Ct	Cycle threshold
CTRL	Control
Da	Dalton
DAPI	4’,6-diamidin-2-phenylindol
DMEM	Dulbecco´s modified eagle medium
DMSO	dimethylsulfoxid
DNA	deoxyribonucleic acid
dNTP	Deoxynucleotide
dpi	Days post-Infection
E. coli	*Escherichia coli*
EDTA	ethylenediaminetetraacetic acid
e.g.	*exempli gratia,* for example
eGFP	enhanced green fluorescent protein
ELISA	enzyme-linked immunosorbent assay
FACS	fluorescence-activated cell sorting
FCS	fetal calf serum
fw	forward
g	gram(s)
g	gravitational force
GAPDH	Glyceraldehyde-3-phosphate dehydrogenase
gp	glycoprotein
h	hour(s)
H_2SO_4	Sulfuric acid
HCl	Hydrochloric acid
HEK293T	human embryonic kidney 293 large T antigen cells
HeLa	Henrietta Lacks
HEPES	4-(2-hydroxyethyl)-1-piperazineethanesulfonic acid
HRP	Horse raddish peroxidase
IC_{50}	50% inhibitory concentration
i.e.	*id est,* in other words
IRES	Internal ribosomal entry site
k	kilo (10^3)

Kana	Kanamycin
KCl	Potassium chloride
kDa	Kilo Daltons
kg	Kilogram
KH_2PO_4	Potassium dihydrogen phosphate
l	liter
LB	lysogeny broth
LSM	laser scanning microscope
m	meter
m	milli (10^{-3})
M	molar (mol/l)
mAb	monoclonal antibody
MEM	minimal essential medium
MFI	mean fluorescence intensity
mg	Milligram
MgCl	Magnesium chloride
MgSO	Magnesium sulfate
min	minute(s)
ml	Milliliter
mm	Millimeter
mRNA	Messenger RNA
MOI	multiplicity of infection
n	nano (10^{-9})
Na_2HPO_4	Disodium hydrogen dehydrate phosphate
NaCl	Sodium chloride
NaOH	Sodium hydroxide
ng	Nanogram
NP40	Nonident P40
ORF	Open reading frame
PAGE	polyacrylamide gel electrophoresis
PBS	phosphate buffered saline
PCR	polymerase chain reaction
PEI	Polyethyleneimine
PFA	paraformaldehyde
pH	*potentia hydrogenii*
PVDF	Polyvinylidene diflouride
qRT-PCR	Real-time-reverse-transcription-PCR
rcf	relative centrifugal force
rev	reverse
RLU/s	relative light units per second
RNA	ribonucleic acid
rpm	revolutions per minute
RPMI	Roswell Park Memorial Institute
rpm	revolutions per minute
RT	reverse transcriptase
s	second(s)
SD	standart deviation
SDS	sodium dodecyl sulfate
S.O.C.	super optimal broth
TAE	tris(hydroxymethyl)aminomethane base, acetic acid, EDTA

TEM	transmission electron microscopy
TMB	3,3',5,5'-tetramethylbenzidine
Tris	trishydroxymethylaminomethane
UV	ultraviolet
V	volt
v/v	volume per volume
VSV	Vesicular stomatitis virus
VSV-G	Vesicular stomatitis virus glycoprotein
w/v	weight per volume
WHO	World Health Organization
WT	Wildtype
β-gal	β-galactosidase

Bases

A	Adenine	T	Thymine	U	Uracil
C	Cytosine	G	Guanine		

One letter amino acid code:

A	Alanine	I	Isoleucine	R	Arginine
C	Cysteine	K	Lysine	S	Serine
D	Aspartic acid	L	Leucine	T	Threonine
E	Glutamic acid	M	Methionine	V	Valine
F	Phenylalanine	N	Asparagine	W	Tryptophan
G	Glycine	P	Proline	Y	Tyrosine
H	Histidine	Q	Glutamine		

1. INTRODUCTION

1.1 COVID-19, a new zoonotic disease

Zoonotic events occurred regularly in human history and are the origin of some of the most devastating human diseases. Approximately 61% of all known human pathogens and transmissible disease causatives are zoonotic and can be transmitted between humans and animals (Taylor et al., 2001), including bacteria, fungi, parasites and prions. Moreover, highly pathogenic viruses like Ebola, avian and swine Influenza, rabies, Zika, West Nile and the Japanese encephalitis virus can be found in animal reservoirs and regularly cross the species border to humans. HIV-1 crossed the species barrier at least four, and HIV-2 at least nine times, with HIV-1 M being the causative agent of today's AIDS pandemic (Faria et al., 2014; Sharp & Hahn, 2011). Zoonosis is fostered by the interaction between Humans and reservoir-carrying animals. There have been several attempts to contain zoonotic pathogens in their animal reservoir by vaccination (Alharbi et al., 2019; Maki et al., 2017). However, what makes the regular occurrence of new zoonoses unavoidable is that reservoirs of zoonosis-associated pathogens are almost impossible to eradicate in the wild (Carlson et al., 2022; Chakraborty et al., 2013).

Coronaviruses (CoV) are enveloped, positive-stranded RNA viruses that have been identified in all four classes of land vertebrates (Chu et al., 2011). It has been suggested that all seven described human CoV originated from zoonotic transmissions (Ye et al., 2020). Two α-CoV (229E and NL63) and two β-CoV (OC43 and HKU1) are responsible for up to 30% of mild respiratory tract infections associated with the symptoms of the common cold (Corman et al., 2018a). Genomic analyses indicate that OC43 and 229E have been endemic in the human population for several decades, if not hundreds of years (**Fig. 1**) (Forni et al., 2021). While possible intermediary hosts are still under debate, bats are the original animal reservoir of 229E and NL63, while OC43 and HKU-1 likely emerged from rodent endemic CoV strains (Corman et al., 2018b).

The first recognized emergence of a β-CoV causing Severe Acute Respiratory Syndrome (SARS) happened among food and animal handlers in November 2002 in the Guangdong (GD) province in China (Skowronski et al., 2005; Xu et al., 2004a). In contrast to the human endemic viruses causing common colds, SARS-CoV-1 is associated with severe neurotrophic, hepatotropic, nephrotropic symptoms. SARS-CoV was described to replicate in both respiratory and enteric tracts as well as in the nervous system causing severe disease

(Ding et al., 2004; Lau et al., 2004; Leung et al., 2003; Xu et al., 2004b). Infection of over 8.000 people from 29 different countries throughout the pandemic lead to over 800 deaths (World Health Organization, 2003). Already during the pandemic, the zoonotic origin of SARS-CoV was traced back to bats and civets as the intermediate host (L. F. Wang & Eaton, 2007; Xu et al., 2004a).

The Middle East Respiratory Syndrome-related Coronavirus (MERS-CoV) was first isolated from a resident of Jeddah, located on the Arabian peninsula, in 2012 (Saey, 2013; Zaki et al., 2012). Regular transmissions from animal hosts to humans with sporadic human-to-human transmissions were observed from 2013 to today (Ramadan & Shaib, 2019). Infection of humans was soon associated with domestic dromedary camels in whom MERS-related CoV are endemic (Alagaili et al., 2014; Haagmans et al., 2014). Similar to SARS-CoV-1, MERS is associated with severe inflammation of the respiratory and enteric tract. With 33% lethality, MERS causes the highest mortality rates of all human coronaviruses (A. R. Zhang et al., 2021).

In December 2019 a new SARS-associated CoV, termed SARS-COV-2, was identified in humans. Early genetic analysis allowed to separate the causative agent of the new COVID-19 disease from former emerging CoVs, as it shares only 79 % sequence identity with SARS-CoV-1 (Wu et al., 2020; P. Zhou et al., 2020a). Compared to SARS-CoV-1 and MERS-CoV, SARS-CoV-2 is typically causing milder disease and is associated with lower mortality (O'Driscoll et al., 2021). The ability to spread from human to human before the onset of symptoms contributed to the rapid global spread of this virus (Jones et al., 2021). Since its initial zoonotic transmission, SARS-CoV-2 has infected more than 535 million people by June 2022 and caused over 6.3 million deaths worldwide (https://covid19.who.int/), being responsible for an ongoing global health and socioeconomic crisis.

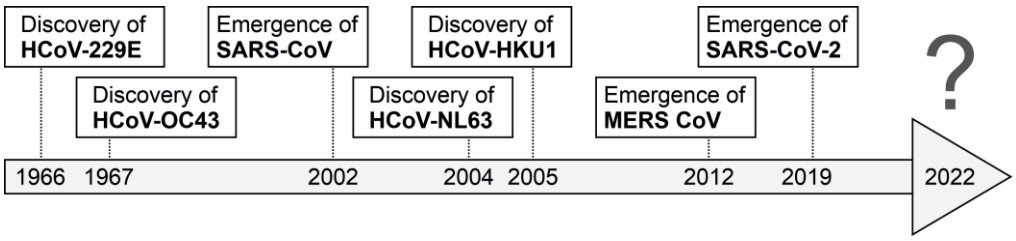

Figure 1: Discovery and emergence of human pathogenic CoV. Shown is a timeline of the discovery and emergence of the seven Coronaviruses in the human population. While HCoV-229E, -OC43, NL63 and -HKU1 were endemic in humans before their discovery, the highly pathogenic SARS-CoV-1, MERS-CoV and SARS-CoV-2 crossed the species barrier within the last 20 years.

1.2 SARS-CoV-2 emerged from bats in Southeast Asia

Early after its emergence, SARS-CoV-2-related CoVs were identified in bats (P. Zhou et al., 2020a). Especially bats in Southeast Asia carry viruses, which share high similarities to SARS-CoV-2 and can potentially infect humans (Figure 2) (Wacharapluesadee et al., 2021; N. Wang et al., 2019). Early in 2012, miners working in caves in the Yunan province of China developed severe pneumonia but were tested negative for most suspected viruses, including SARS-CoV-1. During the following years, fecal samples from bats living in the cave system were collected, leading to the identification of several hundred Sarbeco alpha- and beta-CoV sequences. RaTG13 is one of those bat-associated CoVs that already have been sampled in 2013 from *Rhinolophus (R.) affinis* droppings (Ge et al., 2016; P. Zhou et al., 2020b). With 96.1% sequence identity to the original Wuhan SARS-CoV-2 sequence, RaTG13 represents one of the closest relatives to the pandemic human pathogen identified in bats (Temmam et al., 2021; P. Zhou et al., 2020a). Coronaviruses are notorious for recombination, and while RaTG13, throughout its sequence, is closely related to SARS-CoV-2, parts of the SARS-CoV-2 Spike (S) protein are closer related to sequences of Pangolin CoVs than to RaTG13 S. This led to the hypothesis that pangolins might have served as intermediary hosts during the zoonotic transmission (Lam et al., 2020a; P. Liu et al., 2020). Since the emergence of SARS-CoV-2, several studies have identified Sarbecoviruses in bats, all over Southeast Asia (Wacharapluesadee et al., 2021) (**Fig. 2**), including BANAL-52 in Laos, with 96.6% the closest animal relative of SARS-COV-2 identified to date (Temmam et al., 2022).

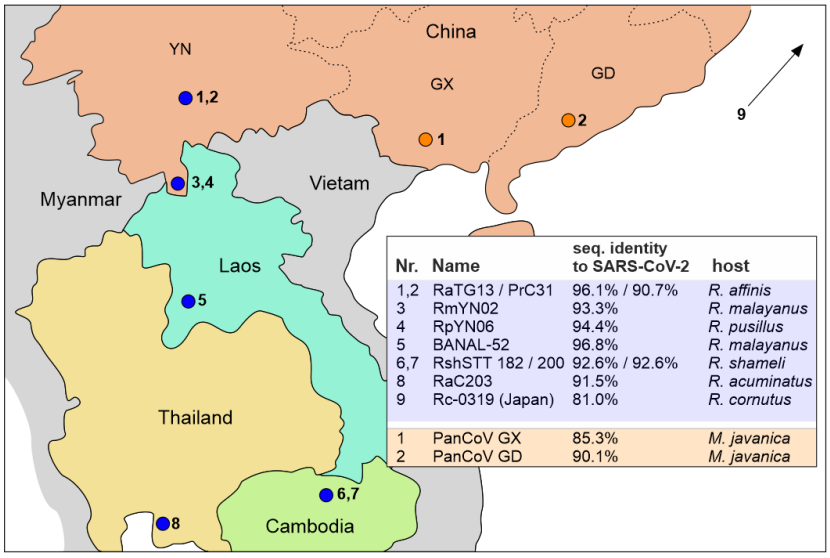

Figure 2: SARS-CoV-2 related Sarbecoviruses were identified in bats and pangolins in Southeast asia. Sarbecoviruses sharing >80% sequence identity to the original SARS-CoV-2 Hu-1 sequence have been identified in China (orange), Laso (turquoise), Thailand (yellew), Cambodia (green) and Japan (not shown).

1.2.1 The versatile CoV Spike proteins

1.2.2 Structure of the CoV Spike and initial human adaptions

Like for all Coronaviruses, the SARS-CoV-2 S protein is a class-I fusion protein synthesized as a 180 kDa precursor and processed into a receptor recognizing S1 and fusion mediating S2 domain. (**Fig. 3**). The S1 domain contains the structural N-terminal domain (NTD), providing a scaffold and directs the receptor-binding domain (RBD) toward the primary ACE2 receptor. The RBD with its core, the Receptor Binding Motiv (RBM), interacts with the cellular receptor and therefore determines cell tropism of the coronavirus (Zhu et al., 2021). S2 contains the N-terminal fusion peptide (FP), anchoring the viral particle to the host cell membrane. Two heptad repeats (HR1/HR2) provide the driving force of fusion and a C-terminal transmembrane domain (TM). (Huang et al., 2020; Zhu et al., 2021). During particle formation, 26 ±15 S trimers are randomly distributed on the virion (Ke et al., 2020; Yao et al., 2020). Activation of the SARS-CoV-2 S is Furin and transmembrane Serinprotease 2 (TMPRSS2) or Cathepsin H/L dependent (Hoffmann & Pöhlmann, 2021b). Furin primes S for further processing by cleaving at the S1/S2 site. During the entry process, TMPRSS2 processes the S2' cleavage site directly upstream of the FP, leading to FP liberation and allowing anchoring of the FP into the cellular membrane (Bestle et al., 2020). The alternative endosomal pathway allows cleavage of the S2' by Cathepsin L after endosomal uptake of the virus (Ke et al., 2020).

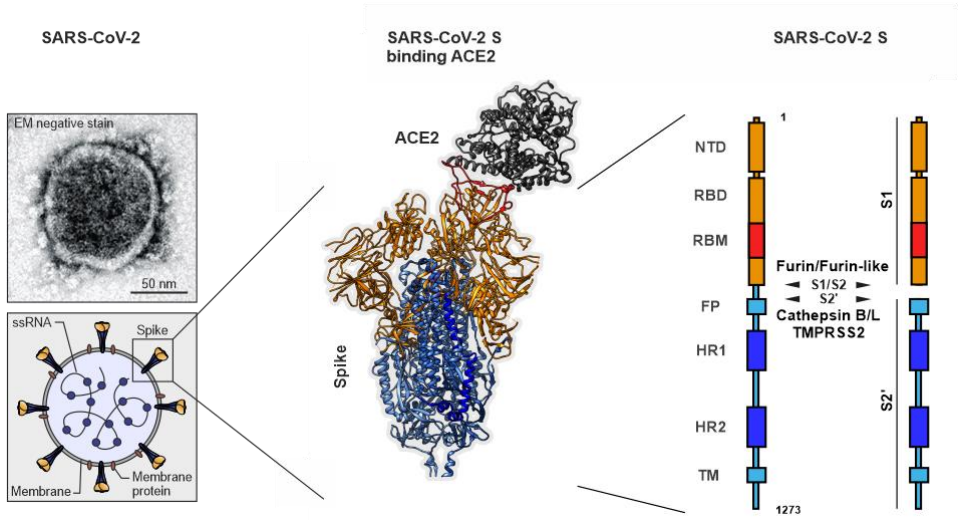

Figure 3: Schematic representation of SARS-CoV-2 and S processing. The SARS-CoV-2 particle as EM negative stain (kindly provided by Clarissa Read, Ulm University) and schematic (left). SARS-CoV-2 Hu 1 based on PDB: 7KNB (middle), domains are indicated in different colors. Receptor binding domain (RBD), orange. Receptor binding motif (RBM), red. Transmembrane domain (TM), light blue. Schematic representation of SARS-CoV-2 and its subunits (right) S1/S2 and S2′ cleavage sites are indicated.

Since the beginning of the SARS-CoV-2 pandemic, researchers have investigated the S protein for traces of human adaptation, allowing SARS-CoV-2 to become the pandemic virus it is today. Mutations that manifest themselves often become defining mutations of new SARS-CoV-2 variants and either provide benefits for replication or, observed more recently in case of the omicron variant of concern (VOC), facilitate immune evasion (Jung et al., 2022; Pastorio et al., 2022). One of the earliest described human adaptions being a novel ^{680}SPRRAR↓SV^{687} furin cleavage site, which enhanced S proteolytic activation and subsequent spread in humans (Peacock et al., 2021). Other human adaptions, like the mutation D614G, led to enhanced ACE2 binding (Plante et al., 2021; Yurkovetskiy et al., 2020; L. Zhang, Jackson, Mou, Ojha, Rangarajan, et al., 2020). P681H/R, a shared defining mutation of the Alpha, Delta and Omicron strains, benefits S proteolytic activation and increases infectivity (Saito et al. 2021). However, a key prerequisite for successful spread of SARS-CoV-2 in the human population was its ability to utilize the human ACE2 receptor for cell entry (Hoffmann, Kleine-Weber, Schroeder, et al., 2020a, 2020b; W. Li et al., 2003; Walls et al., 2020a). Initially, ACE2 binding was considered a key barrier to human spillover (W. Li et al., 2005; Song et al., 2005), promoting the idea of the necessity of an intermediate host. However, almost a decade after the SARS-CoV-1 pandemic, primary isolates from bats were identified that can utilize both, bat and human ACE2 for entry (Ge et al., 2013). A finding that questioned the need of intermediary hosts during CoV related zoonotic events. If a intermediary host was involved during the spillover of SARS-CoV-2 remains under debate.

While sharing over 96% sequence with SARS-CoV-2 S, the RaTG13 S protein poorly binds human ACE2 (K. Liu, Pan, et al., 2021a; Wrobel et al., 2020). After the combined exchange of six amino acid alterations between RaTG13 and SARS-CoV-2 in the RBM, RaTG13 S mediated infection increased by two fold (K. Liu, Ang, et al., 2021). The cellular receptor of RaTG13 in bats is currently unknown.

1.2.3 The Spike protein, a target for drugs and a template for vaccines

Shortly after the first SARS-CoV-2 sequence Wuhan-Hu-1 (MN908947.3) was made public, VSV particle-based pseudovirus assays allowed to determine ACE2 as the SARS-CoV-2 cellular receptor (Hoffmann, Kleine-Weber, Schroeder, et al., 2020b). Since then, pseudovirus-based assays have become an important tool to determine neutralizing titers of

sera from vaccinated individuals, to develop neutralizing antibody therapies, and to evaluate immune escape of novel emerging SARS-CoV-2 VOCs (Hoffmann et al., 2021).

The S protein of SARS-CoV-2 is a suitable target for drugs. In fact, the first FDA-approved medications against SARS-CoV-2 were based on antibodies targeting the S protein. First treatments based on convalescent sera have later been shown to lack beneficial effect on the progression of SARS-CoV-2 infection, as hospitalized patients already have high titers of neutralizing antibodies (Gharbharan et al., 2021; V'kovski et al., 2021). Shortly thereafter, combinations of monoclonal antibodies targeting the RBD domain of the S protein, like Imdevimab, Bamlanivimab or Casirivimab (Baum et al., 2020), were developed and proved effective when administered early during infection. However, not only antibody-based molecules can be used to target the SARS-CoV-2 S protein. EK1 was developed as a broadly active pan-coronavirus inhibiting peptide (Xia et al., 2019). It binds the HR1 region of S, interfering with its ability to mediate host membrane fusion. HR1 is highly conserved in structure and function throughout the Coronavirus family and EK1 derivatives were active against all four common cold CoV, as well as SARS-CoV-1, MERS-CoV and SARS-CoV-2 (Walls et al., 2020b; Xia et al., 2019)

It soon became clear that large-scale immunization of the population was needed to slow down and weaken the detrimental effects of the SARS-CoV-2 pandemic. First vaccines against SARS-CoV-2 were approved by the FDA and the European Commission as early as 10 months after SARS-CoV-2 was announced a pandemic virus, making it the fastest vaccine development in human history (Krammer, 2020). Thereby, the worldwide most distributed vaccines are utilizing a wide range of mechanisms to induce the SARS-CoV-2 neutralizing immune response, ranging from inactivated virus: CoronaVac (Sinovac) & Covaxin (Bharat Biotech), (Palacios et al. 2020; Desai et al. 2022), a variety of adeno-associated viruses as vectors: Vaxzevria/Covishield (Astra Zeneca) & Sputnik V (Gamaleya Institute) (Falsey et al., 2021; Logunov et al., 2021), purified S protein incorporated in nanoparticles (Heath et al., 2021) and also the relatively new mRNA vaccine technology: Comirnaty (Pfizer/BioNTec) & Spikevax (Moderna) (Baden et al., 2021; Polack et al., 2020). By July 2022 vaccines from over 35 manufacturers have been approved in 197 countries (COVID19 Vaccine Tracker) and 64% of the world population has received at least one dose of the COVID-19 vaccine (Mathieu et al., 2021).

A high percentage of vaccinated or reconvalent individuals in the population are benefitting the emerge of SARS-CoV-2 variants, like the omicron VOC, trading pathogenicity for

immune evasion (Jung et al., 2022). As the first companies now started trials on VOC-adapted COVID-19 vaccines and the virus increasingly behaves human endemic (Forni et al., 2021), one should not forget about the zoonotic origin of SARS-CoV-2 and the massive animal reservoir of SARS- and MERS-related CoVs endemic in bats and wildlife stock in Southeast Asia and the Middle East.

1.3 Scope of the study

SARS-CoV-2, the causative agent of the COVID-19 pandemic, emerged either directly or with an intermediate host from bats. RaTG13 was sequenced from droppings of *Rhinolophus affinis* in a mining cave in Yunan, China and shares over 96% sequence identity to SARS-CoV-2. However, the RaTG13 S protein interacts poorly with the human SARS-CoV-2 receptor ACE2 and does not mediate efficient infection of human cells.

Here, it is examined a key alteration that is required to allow the RaTG13 S protein to use human ACE2 for efficient entry into human cells.

Vaccines have proven safe and efficient in the fight against the SARS-CoV-2 pandemic. The antibody response following COVID-19 vaccination is directed against a wide variety of epitopes in the SARS-CoV-2 S protein. It is further examined if vaccination protects us against novel distantly related coronaviruses and future zoonotic events.

2. MATERIALS & METHODS

2.1 Materials

2.1.1 Eukaryotic cells

HEK293T	Adherent human embryonic kidney cell line, transformed by adenovirus type 5 expressing simian virus 40 (SV40) large T-antigen. This cell line, used to produce retroviral particles, was obtained from the American Type Culture Collection (ATCC).
Caco 2	Human epithelial lung adenocarcinoma cells, derived from metastatic site pleural effusion. Provided kindly by Prof. Barth (Ulm University)
Calu-3	Human epithelial lung adenocarcinoma cells were obtained from the ATCC
A549	Human adenocarcinomic alveolar basal epithelial cells provided and validated by Prof. Pöhlmann, German Primate Center, Göttingen
A549 TMPRSS2	Human adenocarcinomic alveolar basal epithelial cells stably expressing TMPRSS2, provided and validated by Prof. Pöhlmann, German Primate Center, Göttingen
A549 ACE2	Human adenocarcinomic alveolar basal epithelial cells stably expressing ACE2, provided and validated by Prof. Pöhlmann, German Primate Center, Göttingen
A549 ACE2/TMPRSS2	Human adenocarcinomic alveolar basal epithelial cells stably expressing ACE2, provided and validated by Prof. Pöhlmann, German Primate Center, Göttingen
I1 Hybridoma	Mouse I1 Hybridoma CRL-2700 were obtained from the ATCC
Tb 1 Lu	Tadarida brasiliensis derived lung epithelial were provided and validated by Marcel A. Müller, Charité-Institute of Virology, Berlin
Ri 1 Lu huACE2	*Rhinolophus affinis* derived lung epithelial cells expressing human ACE2 were provided and validated by Marcel A. Müller Charité-Institute of Virology, Berlin

2.1.2 Primary cells and tissue

human stem cells	For human stem cells used to generate gut organoids: Robert-Koch Institute: Approval according to the stem cell law 29.04.2020/AZ 3.04.02/0084. a more detailed description can be found in the Materials & Methods section of the manuscript.

2.1.3 Bacteria

Escherichia coli XL-2 blue™	*recA1 endA1 gyrA96 thi-1 hsdR17 supE44 relA1 lac* [F' *proAB* lacI^{q}ZΔM15 *Tn*10 (Tet^{r}) Amy Cam^{r}] (Agilent Technologies)
Escherichia coli XL-2 blue MRF'	Δ*(mcrA)183* Δ*(mcrCB-hsdSMR-mrr)173 endA1 supE44 thi-1 recA1 gyrA96 relA1 lac* [F´ *proAB* lacI^{q}ZΔM15 *Tn*10 (Tet^{r})] (Agilent Technologies)]

2.1.4 Viruses

VSVΔG-eGFP	kindly provided by Prof. Klaus Konzelmann, Gene Center Munich
BetaCoV/France/IDF0372/2020	European Virus Archive, Ref-SKU # 014V-03890

2.1.5 Nucleic acids

pCG_SARS-CoV-2 spike C-V5-tag (codon-opt.HUM) IRES eGFP

pCG_SARS-CoV-2 spike R403T C-V5-tag (codon-opt.HUM) IRES eGFP

pCG_PanCovGX spike C-V5-tag (codon-opt.HUM) IRES eGFP

pCG_batCoV-RaTG13-spike C-V5-tag (codon-opt.HUM) IRES eGFP

pCG_batCoV-RaTG13-spike T403R C-V5-tag (codon-opt.HUM) IRES eGFP

pCG_batCoV-RaTG13-spike T403A C-V5-tag (codon-opt.HUM) IRES eGFP

pCG_SARS-CoV-1-spike C-V5-tag (codon-opt.HUM) IRES eGFP

pCG_MERS-CoV-spike C-V5-tag (codon-opt.HUM) IRES eGFP

pCG_NL63-CoV-spike C-V5-tag (codon-opt.HUM) IRES eGFP

pCG_OC43-CoV-spike C-V5-tag (codon-opt.HUM) IRES eGFP

pCG_229E-CoV-spike C-V5-tag (codon-opt.HUM) IRES eGFP

pCG_HKU1-CoV-spike C-V5-tag (codon-opt.HUM) IRES eGFP

pNL1_HIV-1 NL4-3-X4-Δenv f-Luc

All used plasmids contain an ampicillin or kanamycin resistance gene for selection in bacteria.

2.1.6 Primers

Name	Sequences 5' to 3'
RaTG13-spike_fwd	CGTCTAGAATGTTCGTGTTCCTGGTGCTGC
RaTG13-spike_rev	GCACGCGTCTACGTAGAATCGAGACCGAGGAGAGGGTTAGG GATAGGCTTACCACCAGAACCGGTGTAGTGCAGCTTCACGC CCTTC
SARS-COV-2_S_fwd:	CGTCTAGAATGTTTCTGCTGACCACCAAGCGGACCATG
SARS-COV-2_S_V5_rws:	GCACGCGTCTACGTAGAATCGAGACCGAGGAGAGGGTTAGG GATAGGCTTACCACCAGAACCGGTGTAGTGCAGTTTCACGC CCTTC
RaTG13-S_T403R	CTTCGTGATCCGCGGCGACGAGG
RaTG13-S_T403A	CTTCGTGATCGCAGGCGACGAGG
SARS-CoV2-S_ R403T	CTTCGTGATCACCGGAGATGAAGTGCGG
ACE2 fwd	CTTCTAGAATGTCAAGCTCTTCCTGGCTCC
ACE2 RWS	CGACGCGTCTAAAAGGAGGTCTGAACATCATCAGTG
ACE2_E37A fwd	CAAGTTTAACCACGAAGCCGCAGACCTGTTCTATCAAAGTTC ACTTGC
ACE2_E37A rws	GCAAGTGAACTTTGATAGAACAGGTCTGCGGCTTCGTGGTTA AACTTG
ACE2_D38A fwd	CAAGTTTAACCACGAAGCCGAAGCACTGTTCTATCAAAGTTC ACTTGC
ACE2_D38A rws	GCAAGTGAACTTTGATAGAACAGTGCTTCGGCTTCGTGGTTA AACTTG
ACE2_E37-D38AA fwd	CAAGTTTAACCACGAAGCCGCAGCACTGTTCTATCAAAGTTC ACTTGC
ACE2_E37-D38AA rws	GCAAGTGAACTTTGATAGAACAGTGCTGCGGCTTCGTGGTTA AACTTG

2.1.7 Antibodies

α-SARS-CoV-2 N	Sino Biologicals #40588-V08B (1:1000)
α-SARS-CoV-2 S (1A9)	GeneTex #GTX632604 (1:1000)
α-ACE2	Abcam, #ab166755
α-V5	Cell Signaling #13202

VSV-M (23H12)	Absolute Antibody, #Ab01404-2.0 (1:2000)
Anti-HSP70	Santa Cruz W27/sc-24 (1:1000)
Anti-GFP	GenScript A01704-40 (1:1000)
Anti-mouse-647	Invitrogen A31571 (1:2000)
Anti-rabbit-647	Invitrogen A21206 (1:2000)
α-GAPDH	Biolegend #631401 (1:5000)
α-Rabbit IgG PE (H+L)	Abcam ab97070 (1:50)
α-Mouse IgG PE (H+L)	Thermo Fischer Cat#1875522 (1:50)
α-Rabbit IgG (H+L)	HRP Thermo Fischer Cat#32460 (1:20000)
α-Mouse IgG (H+L)	HRP Thermo Fischer Cat#32430 (1:20000)
α-Rabbit IgG (H+L) AF 488	Thermo Fischer Cat#A32731(1:20000)
α-Mouse IgG (H+L) AF 488	Thermo Fischer Cat#A32723(1:20000)
α-Mouse IgG (H+L), AF 647	Thermo Fischer Cat#A-31571(1:20000)
IRDye® 800CW Goat anti-Mouse IgG	Li-CORE, Cat#926-32210
IRDye® 800CW Goat anti-Rat IgG	Li-CORE, Cat#926-32219
IRDye® 680CW Goat anti-Rabbit IgG	Li-CORE, Cat#925-68071
IRDye® 680CW Goat anti-Mouse IgG	Li-CORE, Cat#926-68070
IRDye® 800CW Goat anti-Rabbit IgG	Li-CORE, Cat#926-32211

2.1.8 Enzymes

Trypsin-EDTA 0.5% (10x)	Thermo Fisher Scientific
Alkaline phosphatase	Roche
T4 DNA Ligase	Takara Bio Inc.
Restriction endonucleases	NEB enzymes (Frankfurt)
TAKARA SOL I	Takara Bio Inc.

2.1.9 Buffers

Calcium Chloride Transfection

10x HBS	8.18% (w/v) NaCl, 5.94% (w/v) HEPES and 0.2% (w/v) Na_2HPO_2 in H_2O
2x HBS	10x HBS diluted five-fold with H_2O, adjusted to pH 7.12, sterilized by filtration

2 M $CaCl_2$	prepared with distilled H_2O
SDS PAGE	
Running buffer (1x)	NuPAGE MES SDS (20x) diluted in distilled H_2O
Western Blot	
Transfer buffer	47.9 mM Tris, 38.6 mM glycine, 1.3 mM SDS and 20% (v/v) methanol in distilled H_2O (final pH 8.3)
Antibody buffer	0.2% (v/v) Tween 20, 1% (w/v) milk powder in PBS
Blocking buffer	0.2% (v/v) Tween 20, 5% (w/v) milk powder in PBS
Washing buffer	0.2% (v/v) Tween 20 in PBS
Flow cytometry	
FACS buffer	1% FCS in PBS
Permeabilization solution	300 mM sucrose, 3 mM $MgCl_2$, 50 mM NaCl, 20 mM Tris, and 0.5% (v/v) Triton X-100 in H_2O
Washing and antibody buffer	0.1% (v/v) Tween 20 in PBS
Agarose gel electrophoresis	
50x TAE buffer	2 M Tris-HCl, 1 M acetic acid and 0.1 M EDTA (final pH 8.3)
Agarose gel loading buffer	0.25% (w/v) bromophenol blue, 0.25% (w/v) xylene cyanol, 30% (v/v) glycerol in TAE buffer

2.1.10 Media

Bacteria culture media	
LB agar	1.5% (w/v) agar with 0.01% (w/v) ampicillin or kanamycin in LB medium
LB medium	1% (w/v) bacto tryptone, 0.5% (w/v) bacto yeast extract, 0.8% (w/v) NaCl, 0.1% (w/v) glucose, and 0.01% (w/v) ampicillin or kanamycin added prior to use
S.O.C. medium	Thermo Fisher Scientific
Cell culture media	
DMEM culture medium	Dulbecco's Modified Eagle Medium (DMEM) supplemented with 10% (v/v) heat-inactivated fetal calf serum, 2 mM L-glutamine, 100 units/ml penicillin, and 100 µg/ml streptomycin.

RPMI-1640 culture medium	RPMI-1640 supplemented with 10% (v/v) heat-inactivated fetal calf serum, 2 mM L-glutamine, 100 units/ml penicillin, and 100 µg/ml streptomycin.
MEM culture medium	Minimal essential medium (MEM) supplemented with 10% (v/v) heat-inactivated fetal calf serum, 2 mM L-glutamine,1x non-essential amino acids, 100 units/ml penicillin, and 100 µg/ml streptomycin.
ECM culture medium	RPMI-1640 supplemented with 13% (v/v) heat-inactivated fetal calf serum, 2 mM L-glutamine, 1 mM sodium pyruvate, 1x non-essential amino acids, 100 units/ml penicillin, 100 µg/ml streptomycin, 100 µg/ml gentamicin, and 2.5 µg/ml amphotericin B

2.1.11 Reagents

1 kilo base pair Plus DNA Ladder	Thermo Fisher Scientific
4′,6-Diamidino-2-phenylindole dihydrochloride (DAPI)	Sigma-Aldrich
Agar	BD Biosciences
Agarose	Thermo Fisher Scientific
Ampicillin	Ratiopharm
Bacto tryptone	Becton Dickinson
Bacto yeast extract	Becton Dickinson
Calcium chloride dihydrate	PanReac AppliChem
Dimethylsulfoxid	Merck KGaA
Distilled H_2O (HPLC grade)	VWR
Dulbecco's Modified Eagle Medium (DMEM)	Thermo Fisher Scientific
Ethanol (99.8% purity)	VWR
Ethidium bromide	PanReac AppliChem
FACS clean solution	BD Biosciences
FACS flow solution	BD Biosciences
FACS shutdown solution	BD Biosciences
Fetal bovine/calf serum (FCS)	Thermo Fisher Scientific
fixable viability stain 450 (FVS)	BD Biosciences
Glucose	Merck KGaA

Glutaraldehyde	PLANO
HEPES	Sigma-Aldrich
Hypochlorite (1%)	PanReac AppliChem
Immobilon-FL™ Transfer Membrane	Millipore
Isopropanol	VWR
Kanamycin Sulfate	Thermo Fisher Scientific
L-Glutamine	Thermo Fisher Scientific
Methanol	Sigma-Aldrich
$MgCl_2$	Merck KGaA
minimal essential medium (MEM)	Thermo Fisher Scientific
Non-essential amino acids	Sigma-Aldrich
NuPAGE™ MES SDS Running Buffer	Thermo Fisher Scientific
NuPAGE™ Novex 4-12% Bis-Tris Gel 1.0 mm	Thermo Fisher Scientific
Paraformaldehyde	Merck KGaA
Penicillin-Streptomycin	Thermo Fisher Scientific
Phosphate buffered saline (PBS), no calcium, no magnesium	Thermo Fisher Scientific
Potassium chloride (KCl)	PanReac AppliChem
Potassium dihydrogen phosphate (H_2KO_4P)	PanReac AppliChem
Precision Plus™ Protein Kaleidoscope Standard	Bio-Rad
Protein Loading Buffer	LI-COR
Roswell Park Memorial Institute medium (RPMI-1640)	Thermo Fisher Scientific
Sodium chloride (NaCl)	Sigma-Aldrich
Sodium dihydrogen phosphate (NaH_2PO_4)	Sigma-Aldrich
Sodium hydrogencarbonate ($NaHCO_3$)	Sigma-Aldrich
Sodium hydroxide (NaOH)	Merck KGaA
Sodium pyruvate	Thermo Fisher Scientific
Sucrose	Carl Roth
Sulfuric acid (H_2SO_4)	Merck KGaA
TAE buffer	5Prime
Thioflavin T (ThT)	Sigma-Aldrich
Triton X-100	Sigma-Aldrich
Tween® 20	Sigma-Aldrich
Uranyl acetate	Merck KGaA

β-mercaptoethanol	Sigma-Aldrich

2.1.12 Consumables

Cell culture flasks	Sarstedt
Cryo tubes	Sarstedt
FACS tubes	BD Biosciences
Folded capillary cell DTS 1061	Malvern
Gloves	VWR
Greiner FLUOTRAC™ 600 black 96 well plates	Sigma-Aldrich
Nunc-Immuno™ MicroWell™ MaxiSorp™ 96 well flat plate	Sigma-Aldrich
Pipette tips	Sarstedt
Protran BA85 Nitrocellulose Blotting Membrane	GE Healthcare
Reaction tubes 1.5 ml	Sarstedt
Reaction tubes 2.0 ml	Sarstedt
Reagent reservoirs	VWR
Serological pipettes	Sarstedt
Stericup Filter Unit 0.45 µm	Millipore
Syringe	BD Biosciences
TC Plate 24 Well, Standard, F	Sarstedt
TC Plate 6 Well, Standard, F	Sarstedt
TC Plate 96 Well, Standard, F	Sarstedt
TC Plate 96 Well, Standard, R	Sarstedt
TC Plate 96 Well, Standard, U	Sarstedt
Tubes 15 ml	Sarstedt
Tubes 50 ml	Sarstedt
Whatman™ paper	GE Healthcare
White Nunc™ 96 well polystyrene plates	Thermo Fisher Scientific
Wipes	Kimberly-Clark
µ-Slides 8 well	Ibidi

2.1.13 Kits

CellTiter-Glo® Luminescent Cell Viability Assay	Promega
Gal-Screen™ β-Galactosidase Reporter Gene Assay System for Mammalian Cells	Thermo Fisher Scientific

Luciferase Assay System	Promega
ProteoStat® Amyloid Plaque Detection Kit	Enzo Life Sciences
RealStar® Zika Virus RT-PCR Kit	altona Diagnostics
Restriction endonucleases and respective buffers	New England BioLabs
Wizard® Plus Midipreps DNA Purification System	Promega

2.1.14 Technical equipment

Axio-Observer.Z1 fluorescence microscope	Zeiss
BD FACSCanto™ II Cell Analyzer	BD Biosciences
BINDER BD 53 Incubator	Binder
Centrifuge 5417R Rotor: F 45 30 11	Eppendorf
Centrifuge 5804R Rotor: 96 well plate A-2-MTP	Eppendorf
Centrifuge 5810R Rotor: A 4 81	Eppendorf
Discovery comfort 12-channel pipettes	HTL Lab Solutions
Discovery comfort pipettes	HTL Lab Solutions
DM IL LED microscope	Leica microsystems
Electric glow discharger Edwards High Vacuum	Leica Microsystems
FiveEasy™ pH meter	Mettler Toledo
Forma Steri-Cult™ CO_2 incubator	Thermo Fisher Scientific
Gel Doc™ XR System	Bio-Rad
Hemacytometer cover glasses	VWR
Hemacytometer Neubauer improved	VWR
Heracell™ 240 CO_2 incubator	Thermo Fisher Scientific
Herasafe™ KSP laminar flow hood	Thermo Fisher Scientific
HXP 120 C	Pulch + Lorenz
Infinite® M1000 PRO Fluorimeter	Tecan
Invitrogen™ Novex™ XCell™ SureLock™ Mini-Cell	Thermo Fisher Scientific
KERN ABJ 120 4M scale	Kern & Sohn
LASOS® RMC Ar-Ion Laser	LASOS
LSM 710 confocal laser scanning microscope	Zeiss
NanoDrop 2000 UV-Vis Spectrophotometer	Thermo Fisher Scientific
Odyssey® Infrared Imaging System	LI-COR
Orion II Microplate Luminometer	Titertek Berthold
PowerPac™ Basic Power Supply	Bio-Rad

PowerPac™ HC High-Current Power Supply	Bio-Rad
Rotilabo® mini-centrifuge	Carl Roth
Sartorius® CERTOMAT® IS	Thermo Fisher Scientific
Thermomixer comfort	Eppendorf
Titramax 100 plate shaker	Heidolph Instruments
Trans-Blot® Turbo™ Tansfer System	Bio-Rad
UV transilluminator, 366nm	Syngene
VMax Kinetic ELISA Microplate Reader	Molecular Devices
Vortex mixer	VWR
Vortex-Genie 2®	Scientific Instruments
Zeiss EM 10 transmission electron microscope	Zeiss

2.1.15 Software

BD FACSDiva™	BD Biosciences
CorelDRAW X4	Corel
FlowJo 7	FlowJo
GraphPad Prism 5	GraphPad Software
i-control™ – Microplate Reader Software	Tecan
LSM 710 Release version 5.5SP1	Zeiss
Microsoft Office	Microsoft
Odyssey™ Infrared Imaging	LI-COR
Quantity One™	Bio-Rad
Simplicity 4.02	Titertek Berthold
Softmax Pro™	Molecular Devices

2.1.16 Other External facilities

Company	Services provided
Eurofins Genomics	siRNAs, DNA sequencing
Microsynth AG SeqLab	DNA sequencing
Baseclear	Custom nucleotide synthesis

2.2 Methods

2.2.1 Plasmid DNA preparation

Plasmid DNA was prepared by alkaline lysis of grown bacterial cultures using the Wizard® Plus Midiprep Kit as recommended by the manufacturer. Concentration and purity of plasmid DNA was determined using the NanoDrop™ 2000 Spectrophotometer.

2.2.2 Restriction Digest

Correct size of isolated plasmid DNA was analyzed by restriction digest using appropriate endonucleases and buffers according to the New England BioLabs' instructions followed by subsequent gel electrophoresis.

2.2.3 Agarose gel electrophoresis

Plasmid DNA and fragments were separated on a 0.7% (w/v) agarose gel containing ethidium bromide. To this end, 20 µl digested samples were ran in parallel to 5 µl DNA ladder with 20% (v/v) loading dye on the gel in TAE buffer for 30 minutes at 120 V (Voltage PowerPAC Basic Power Supply). DNA bands were visualized with the Gel Doc XR.

2.2.4 Transformation of bacteria

In order to amplify expression and proviral vectors, bacteria were transformed with plasmid DNA. To this end, 0.5 µl of plasmid DNA preparations were incubated with 5 µl *Escherichia coli* XL-2 blue™ or XL-2 blue MRF' (to avoid recombination in plasmids containing proviral T/F HIV-1) for 20 minutes on ice followed by a 30 second heat-shock at 42 °C and another 2.5 minutes of cooling on ice. To stimulate bacterial growth, 200 µl of S.O.C. medium was added to the transformed bacteria and they were incubated for 40 minutes at 37 °C under 400 rpm of shaking in a Thermomixer. After incubation, 70 µl of bacteria was plated on LB agar plates containing appropriate antibiotics (ampicillin or kanamycin) for selection and plates were incubated overnight in an incubator at 37 °C (XL-2 blue) or 30 °C (XL-2 blue MRF').

2.2.5 Culture of bacteria

To amplify transformed bacteria for midi preparations, single colonies of bacteria were cultured in 150 ml LB medium supplemented with 100 mg/L antibiotic (ampicillin or

kanamycin, respectively) and incubated on a shaker for 12-16 hours at 37 °C (XL-2 blue) or for 24 hours at 30 °C (XL-2 blue MRF').

2.2.6 Cell culture

All cells were cultured at 37°C in a 5% CO2 atmosphere. Human embryonic kidney 293T cells purchased from American type culture collection (ATCC: #CRL3216) were cultivated in Dulbecco's Modified Eagle Medium (DMEM, Gibco) supplemented with 10% (v/v) heat-inactivated fetal bovine serum (FBS, Gibco), 2 mM L-glutamine (PANBiotech), 100 µg/ml streptomycin (PANBiotech) and 100 U/ml penicillin (PANBiotech). Calu-3 (human epithelial lung adenocarcinoma, kindly provided and verified by Prof. Frick, Ulm University) cells were cultured in Minimum Essential Medium Eagle (MEM, Sigma) supplemented with 10% (v/v) FBS (Gibco) (during viral infection) or 20% (v/v) FBS (Gibco) (during all other times), 100 U/ml penicillin (PAN-Biotech), 100 µg/ml streptomycin (PAN-Biotech), 1 mM sodium pyruvate (Gibco), and 1 mM NEAA (Gibco). Caco-2 (human epithelial colorectal adenocarcinoma, kindly provided by Prof. Holger Barth, Ulm University) cells were cultivated in DMEM (Gibco) containing 10% FBS (Gibco), 2 mM glutamine (PANBiotech), 100 µg/ml streptomycin (PANBiotech), 100 U/ml penicillin (PANBiotech), 1 mM Non-essential amino acids (NEAA, Gibco), 1 mM sodium pyruvate (Gibco). A549, A549 ACE2, A549 TMPRSS2 and A549 ACE2/TMPRSS2 cells were cultured in DMEM (Gibco) supplemented with 10% (v/v) FBS (Gibco), 100 U/ml penicillin (PAN-Biotech), 100 µg/ml streptomycin (PAN-Biotech) and 10 µg/ml Puromycin for A549 ACE2 and A549 ACE2/TMPRSS2 and 10 µg/ml Blasticidin for A549 TMPRSS2 and A549 ACE2/TMPRSS2. I1-Hybridoma cells were purchased from ATCC (#CRL-2700) and cultured in RPMI supplemented with 10% (v/v) heat-inactivated FBS (Gibco), 2 mM L-glutamine (PANBiotech), 100 µg/ml streptomycin (PANBiotech) and 100 U/ml penicillin (PANBiotech). Tb 1 Lu (Tadarida brasiliensis derived lung epithelial) and Ri 1 Lu huACE2 (Rhinolophus affinis derived lung epithelial cells expressing human ACE2, kindly provided by Marcel A. Müller, were cultured in DMEM supplemented with 10% (v/v) heat-inactivated FBS (Gibco), 2 mM L-glutamine (PANBiotech), 100 µg/ml streptomycin (PANBiotech) and 100 U/ml penicillin (PANBiotech), 2 mM sodium pyruvate (Gibco).

2.2.7 Viruses and viral particles

Viral isolate BetaCoV/France/IDF0372/2020 (#014V-03890) was obtained through the European Virus Archive global. To produce pseudotyped VSVΔG-GFP particles, 6*106

HEK293T cells were seeded 18 h before transfection in 10 cm dishes. The cells were transfected with 15 µg of a glycoprotein expressing vector using PEI (PEI, 1 mg/ml in H2O, Sigma-Aldrich). 24 h post-transfection, the cells were infected with VSVΔG-GFP particles pseudotyped with VSV G at a MOI of 3. One h post-infection, the inoculum was removed. Pseudotyped VSVΔG-GFP particles were harvested 16 h post-infection. Cell debris were pelleted and removed by centrifugation (500 g, 4 °C, 5 min). Residual input particles carrying VSV-G were blocked by adding 10 % (v/v) of I1 Hybridoma Supernatant (I1, mouse hybridoma supernatant from CRL-2700; ATCC) to the cell culture supernatant.
For the production of lentiviral HKU1 S pp, HEK293T cells were transfected with spike expression plasmids together with a pNL1_HIV-1_NL4-3-Δenv-fluc backbone. 48 hours post-transfection, supernatants were harvested and stored at -80°C.

2.2.8 Transfections

Plasmid DNA was transfected using either calcium phosphate transfection or Polyethylenimine (PEI, 1 mg/mL in H2O, Sigma-Aldrich) according to the manufacturer's recommendations or as described previously.

2.2.9 Molecular dynamics simulation

Based on the structure of ACE2-bound to SARS-CoV-2 S taken from the Protein Data Bank (identification code 7KNB), the initial atomic positions were obtained. Equilibration (300K for 0.5 ns) was performed by ReaxFF (reactive molecular dynamic) simulations within the Amsterdam Modeling Suite 2020 (http://www.scm.com). Based on the equilibrated structure, amino acids from the S protein were replaced with the respective amino acids from RaTG13, respectively the modification. After an additional equilibration (300K for 0.5 ns) ReaxFF (reactive molecular dynamic) simulations were performed within the NVT ensemble over 25 ps, while coupling the system to a Berendsen heat bath (T=300 K with a coupling constant of 100 fs). The interaction energy was obtained by averaging over these simulations. For all visualizations the Visual Molecular Dynamics program (VMD) was used.

2.2.10 Whole-cell and cell-free lysates

Whole-cell lysates were prepared by collecting cells in Phosphate-Buffered Saline (PBS, Gibco), pelleting (500 g, 4 °C, 5 min), lysing and clearing as previously described. Total protein concentration of the cleared lysates was measured using the Pierce BCA Protein

Assay Kit (Thermo Scientific) according to manufacturer's instructions. Viral particles were filtered through a 0.45 µm MF-Millipore Filter (Millex) and centrifuged through a 20% sucrose (Sigma) cushion. The pellet was lysed in transmembrane lysis buffer already substituted with Protein Sample Loading Buffer (LI-COR).

2.2.11 SDS-PAGE and immunoblotting

SDS-PAGE and immunoblotting was performed as previously described. In brief, whole-cell lysates were separated on NuPAGE 4-12% Bis-Tris Gels (Invitrogen) for 90 min at 120 V and blotted at constant 30 V for 30 min onto Immobilon-FL PVDF membrane (Merck Millipore). After the transfer, the membrane was blocked in 1% Casein in PBS (Thermo Scientific) and stained using primary antibodies directed against SARS-CoV-2 S (1:1,000, Biozol, 1A9, #GTX632604), ACE2 (1:1,000, Abcam, # ab166755), VSV-M (1:2,000, Absolute Antibody, 23H12, #Ab01404-2.0), V5-tag (1:1,000, Cell Signaling, #13202), GAPDH (1:1,000, BioLegend, #631401) and Infrared Dye labelled secondary antibodies (1:20,000, LI-COR IRDye). Proteins were detected using a LI-COR Odyssey scanner and band intensities were quantified using LI-COR Image Studio.

2.2.12 ACE2 interaction assay

HEK293T Cells expressing the indicated S constructs were collected after 48 hours in Phosphate-Buffered Saline (PBS, Gibco), divided for simultaneous immunoblotting and ACE2 interaction assay and pelleted (500 g, 4 °C, 5 min). For the ACE2 interaction assay, the cells were lysed in NP-40 buffer (150 mM NaCl, 1% (vol/vol) NP-40, 50 mM HEPES pH 7.4 and protease inhibitor cocktail (Sigma)) and cell debris pelleted by centrifugation at 13,000 r.p.m. for 20 min at 4 °C. ACE2 coated wells (COVID-19 S-ACE2 binding assay II, Ray Bio) were incubated for 2 hrs with 50 µl of WCLs and washed extensively with the provided wash buffer (RayBio, #EL-ITEMB). The wells were incubated 1 hr with 100 µl anti-V5(MS) (1:1,000, Cell Signaling, #80076), subsequently washed and incubated for 1 hr with 100 µl anti-MS-HRP (1:1,000, RayBio). After washing, the samples were incubated with 50 µl of TMB Substrate Solution (RayBio, #EL-TMB) for 30 min. The reaction was stopped by adding 50 µl Stop Solution (RayBio, #EL-STOP). Absorption was measured at 450 nm with a baseline correction at 650 nm.

2.2.13 Stem Cell Culture and Intestinal Differentiation

Human embryonic stem cell line HUES8 (Harvard University, Cambridge, MA) was used with permission from the Robert Koch Institute according to the "79. Genehmigung nach dem Stammzellgesetz, AZ 3.04.02/0084." Cells were cultured on human embryonic stem cell matrigel (Corning, Corning, NY) in mTeSR Plus medium (STEMCELL Technologies, Vancouver, Canada) at 5% CO2, 5% O2, and 37°C. Medium was changed every other day and cells were split with TrypLE Express (Invitrogen, Carlsbad, CA) twice a week. For differentiation, 300,000 cells per well were seeded in 24-well plates coated with growth factor–reduced matrigel (Corning) in mTeSR Plus with 10 mM Y-27632 (STEMCELL Technologies). The next day, differentiation was started at 80%-90% confluency, as described previously45.

2.2.14 Intestinal organoids

To prepare in vitro differentiated organoids for transduction, matrigel was dissolved in Collagenase/Dispase (Roche, Basel, Switzerland) for 2 h at 37°C and stopped by cold neutralization solution (DMEM, 1% bovine serum albumin, and 1% penicillin-streptomycin). Organoids were transferred into 1.5-mL tubes and infected in 300 µL pseudoparticle containing inoculum. Organoids were then resuspended in 35-µL cold growth factor–reduced matrigel to generate cell-matrigel domes in 48-well plates. After 10 minutes at 37°C, intestinal growth medium (DMEM F12 [Gibco, Gaithersburg, MD], 1× B27 supplement [Thermo Fisher Scientific], 2-mM L-glutamine, 1% penicillin-streptomycin, 40 mM HEPES [Sigma-Aldrich], 3 µM CHIR99021, 200 nM LDN-193189 [Sigma-Aldrich], 100 ng/mL hEGF [Novoprotein, Summit, NJ], and 10 µM Y-27632 [STEMCELL Technologies]) was added and organoids were incubated at 37°C. The organoids were imaged using the Cytation 3 cell imaging system and processed with Gen 5 and ImageJ software. For FACS preparation, the matrigel was dissolved and the extracted organoids were dissolved in Accutase (Stemcell technologies). The cells were fixed with 1% PFA in PBS for 10 min at 4°C and washed with cold PBS containing 2% FBS. Flow cytometry analyses were performed using a FACS CANTO II (BD) flow cytometer. Transduction rates were determined by GFP expression and analyzed with DIVA and Flowjow10 software.HIV,

2.2.14.1 Pseudoparticle inhibition

VSVpp inhibition experiments were performed as previously described46. In brief, Caco-2 cells were infected with 100 µl freshly produced VSVΔG-GFP pseudo particles, which were preincubated (30 min, 37°C) with the indicated amounts of Casivirimab (REGN10933, orange), EK-1 (Core Facility Functional Peptidomics (UPEP), Ulm University) or Sera of with BNT162b2 vaccinated donors. GFP positive cells were automatically quantified using a Cytation 3 microplate reader (BioTek).

2.2.15 Sera from vaccinated individuals and ethics approval

Blood samples of ChAdOx1-nCoV-19/BNT162b2 and BNT162b2 vaccinated individuals were obtained after the participants information and written consent. Samples were collected 13-30 days after the second dose using S-Monovette Serum Gel tubes (Sarstedt). Before use, the serum was heat-treated at (56°C, 30 min). Ethics approval was given by the Ethic committee of Ulm University (vote 31/21 – FSt/Sta).

2.2.16 Treatment with ATN-161

Caco-2 cells were preincubated with the indicated amounts of α5β5 integrin Inhibitor ATN-161 (Sigma) for 2 h and infected with 100 µl freshly produced VSVΔG-GFP pseudo particles. Sixteen h post-infection, GFP positive cells were automatically quantification using a Cytation 3 microplate reader (BioTek). Calu-3 cells were preincubated with the indicated amounts of ATN-161 (Sigma) for 2 h and infected with SARS-CoV-2 isolate BetaCoV/France/IDF0372/2020 (MOI 0.05, 6 h). 48 h post-infection supernatants were harvested for qRT-PCR analysis.

2.2.17 Sequence logo and alignments.

Alignments of primary bat sequences (GU190215.1, QPD89842.1, KY417145.1, KY938558.1, KU182964.1, KJ473811.1, MN996532.1, KY417152.1, MK211376.1, KY417146.1, KY417150.1, KT444582.1, MG772933.1, MG772934.1, KY770858.1, KY770859.1, KJ473816.1, MK211374.1, JX993987.1, KJ473814.1, DQ648856.1, KY770860.1, KJ473812.1, KJ473813.1, JX993988.1, KY417143.1, MK211378.1, DQ412043.1, DQ648857.1, KY417148.1, MK211375.1, KY417147.1, KY417142.1, MK211377.1, KJ473815.1, GQ153542.1, GQ153543.1, KF294457.1, GQ153547.1, DQ084199.1, GQ153548.1, DQ022305.1, DQ084200.1, GQ153545.1, GQ153546.1, GQ153539.1, GQ153540.1, GQ153541.1, GQ153544.1) were performed using ClustalW

with a gapOpening penalty of 80. Sequence logos were generated using R packages ggplot2 and ggseqlogo.

2.2.18 Statistics

Statistical analyses were performed using GraphPad PRISM 9.2.0 (GraphPad Software). P-values were determined using a two-tailed unpaired Student's t test. Unless otherwise stated, data are shown as the mean of at least three independent experiments ± SEM.

3. RESULTS

3.1 RaTG13 S pp poorly infect SARS-CoV-2 permissive Caco-2 cells

VSVΔG pp infection assays are a well-established method to mimic the entry of various enveloped viral pathogens into their host cells. To investigate entry of the human pathogenic SARS-CoV-2, SARS-CoV and MERS-CoV, as well as the pangolin CoV (PCoV GX) and Bat CoV RaTG13, we pseudotyped VSVΔG eGFP particles with the various S proteins and infected ACE2 expressing colorectal adenocarcinoma (Caco-2) cells (Fig 4a). While ACE2 is the receptor of SARS-CoV, SARS-CoV-2 and PCoV-GX, MERS utilizes the human DPP4 receptor. The human receptor for RaTG13 is unknown, but high sequence similarity between RaTG13 and SARS-CoV-2 made it tempting to speculate that RaTG13 S can also utilize human ACE2 for cell entry. SARS-CoV-2, SARS-CoV-1, PCoV GX and MERS S mediated Caco-2 infection to a simlar extent. However, it came as surprise that RaTG13 S was hardly able to mediate infection of Caco-2 cells and automated quantification of the infection events/well revealed a ~15x drop between SARS-CoV-2 S and RaTG13 S mediated infection events (Fig. 4b)

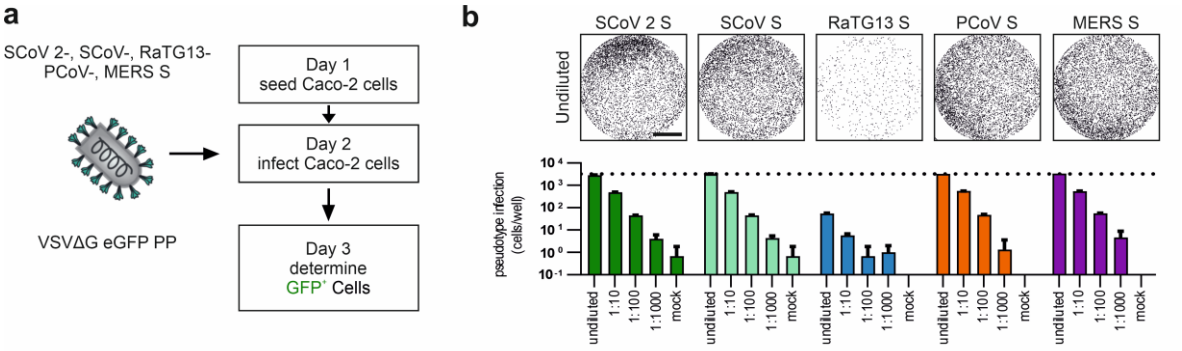

Figure 4: Infection of Caco-2 cells with SARS-CoV-2, SARS-CoV-1, PCoV GX, MERS and RaTG13 S pseudotyped particles. a, Schematic presentation of the assay to assess S-mediated VSVpp infection. **b** Binary images of Caco-2 cells transduced with VSVΔG-GFP pseudotyped with SARS-CoV-2, SARS-CoV-1, RatG13, PCoV GX and MERS S. Successful infection events (=GFP positive cells) displayed as black dots. Scale bar, 1.5mm (upper panel) and automatic quantification of the titration of the indicated pseudotyped particles on Caco-2 clles by counting GFP positive cells. Bars represent the mean of three independent experiments (±SEM) (lower panel).

3.2 SARS-COV-2 S R403 contributes to ACE2 binding

Previously published *in silico* simulations identified S residue R403 to be involved in intramolecular interactions, stabilizing the SARS-CoV-2 S trimer interfaced. To further narrow down interaction partners of R403 in the ACE2 receptor, ReaxFF based

computational modelling was performed. A positively charged residue at position 403 distinguishes the S proteins of PCoV (K403), SARS-CoV-1 (K403) and SARS-CoV-2 (R403) from the bat CoV RaTG13 S protein (T403) (Fig. 5a). Notably, R403 is highly conserved in SARS-CoV-2 S sampled and sequenced from infected humans: only 585 of ~9.5 million S sequences recorded on GSAID contain a conservative change of R403K and just 203 other amino acids.

The modeling further supported S/ACE2 interaction and the establishment of close proximity with putative charge interactions between R403 in the SARS-CoV-2 S and a Glutamic Acid at position 37 (E37) in the human ACE2 receptor (Fig. 5b). The contribution of this interaction was quantified to an average of 3 eV during 150 ps simulation time (Fig. 5c).

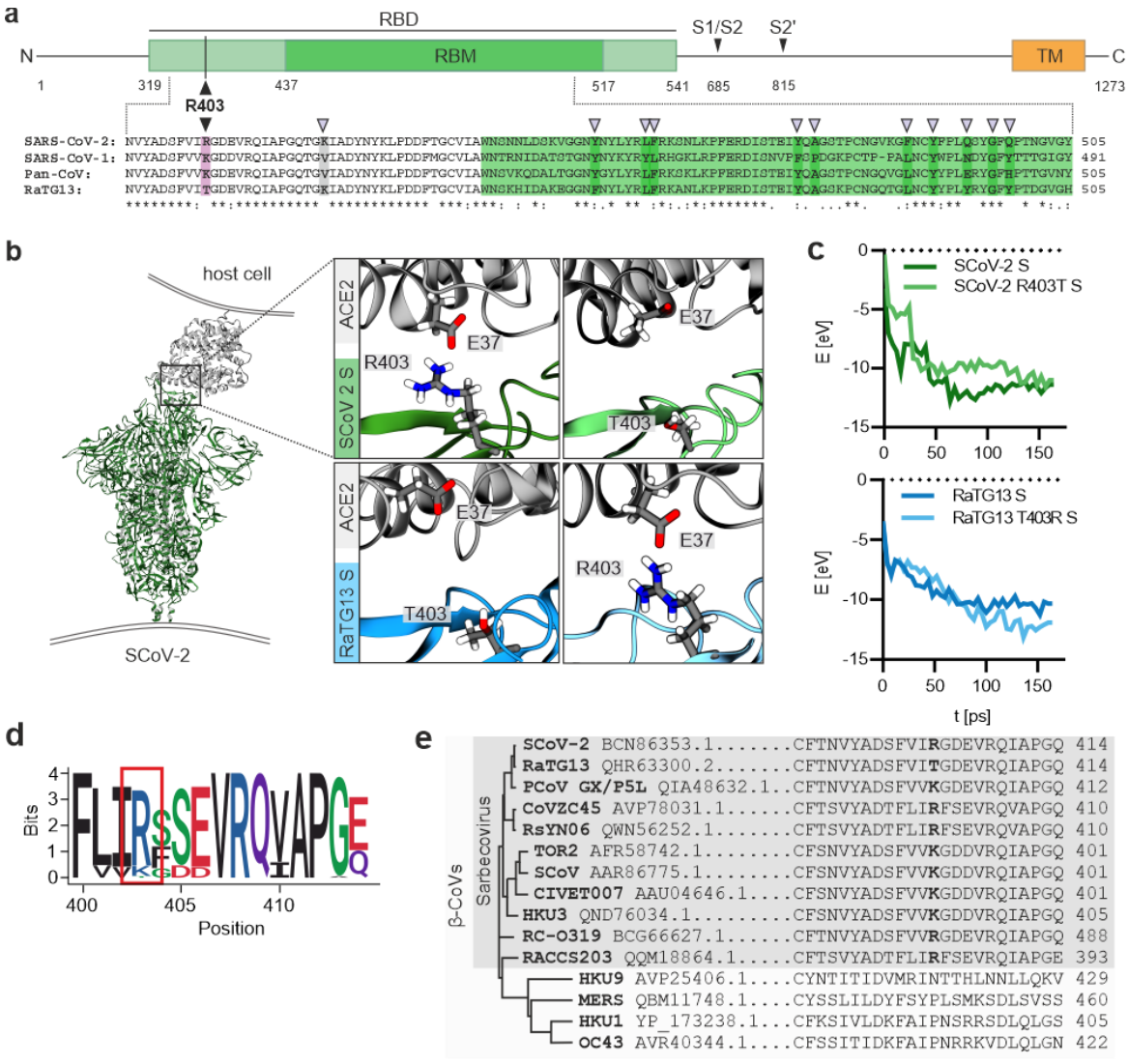

Figure 5: Modelling of the interaction of Coronavirus spike residue 403 with human ACE2. a, Schematic representation of the SARS-CoV-2 S protein (top panel), domains are indicated in different colors. Receptor binding domain (RBD), light green. Receptor binding motif (RBM), dark green. Transmembrane domain (TM),

orange. R403, pink. S1/S2 and S2' cleavage sites are indicated. Sequence alignment of SARS-CoV-2, SARS-CoV-1, Pan-CoV and RaTG13 S RBD (bottom panel). Sequence conservation is indicated. grey arrows denote important residues for ACE2 binding. **b,** Reactive force field simulation of SARS-CoV-2 S in complex with human ACE2 (PDB: 7KNB) (left panel) and focus on position 403 in SARS-CoV-2 S (R) or RaTG13 S (T) or respective exchange mutants at position 403 (right panel). ReaxFF based computational analysis was performed by C. J. **c**, Exemplary energy curve of the reactive molecular dynamics simulation for SARS-CoV-2 S and SARS-CoV-2 S R403T (top panel) and RaTG13 and RaTG13 T430R S with human ACE2 (bottom panel). **d**, Sequence logo of the alignment of 50 different Sarbecovirus S RBD sequences between sequence positions 400 and 414. Position R403 is highlighted by a red box. **e,** Primary sequence alignment of selected bat, pangolin and human CoVs. Position R403 is highlighted in bold. ReaxFF based computational analysis was performed by C. J.. From Zech et al., 2021 CC BY 4.0

3.3 T403R allows RaTG13 spike to use human ACE2 as receptor

To determine the impact of position 403 on S/ACE2 interaction, Caco-2 cells were infected with VSVΔG-eGFP pseudotyped with parental and 403 mutant S proteins. While mutation of R403T reduced the ability of the SARS-CoV-2 S protein to infect Caco-2 cells by 40% (Fig. 6a), the T403R mutation enhanced the infectiousness of RaTG13 VSVpp for Caco-2 cells by ~30-fold. The control, RaTG13 S T403A substitution had no enhancing effect (Fig. 6a). Similar results were obtained in the human lung cancer cell line Calu-3, here the SARS-CoV-2 R403T VSVpp infection was reduced and albeit low infection rates in CaLu-3 cells, RaTG13 S VSVpp infection was increased by ~10-fold (Fig. 6b). VSVpp infection of the lung carcinoma cell line A549 depended on ACE2 and TMPRSS2 expression (Fig. 6c; Supplementary Fig. 1). While ACE2 expression was strictly required for infection, coexpression of TMPRSS2 enhanced infection mediated by the parental and R403T SARS-CoV-2 S proteins by 4 fold, but had no effect on entry mediated by the RaTG13 T403R S (Fig. 6c). Coexpression of parental SARS-CoV-2 S IRES eGFP and human ACE2 IRES eGFP in HEK293T cells resulted in the formation of large syncytia, while parental and T403A RaTG13 S did not induce detectable cell-cell fusion. However, significant syncytia formation was observed for the T403R mutated RaTG13 S (Fig. 6d & 6e). To investigate the inductive effect of R403 in a more physiological system, infection was studied on intestinal organoids derived from human pluripotent stem cells (hPSC). Similar to the effects observed in cell lines, the parental SARS-CoV-2 S protein allowed efficient infection with a slightly reduced infection efficiency in the R403T mutant. Parental and T403A mutated RaTG13 S protein did not mediate VSVpp entry, while the T403R S allowed significant infection of the intestinal organoids (Figs. 6f & 6g, Supplementary Fig. 2).

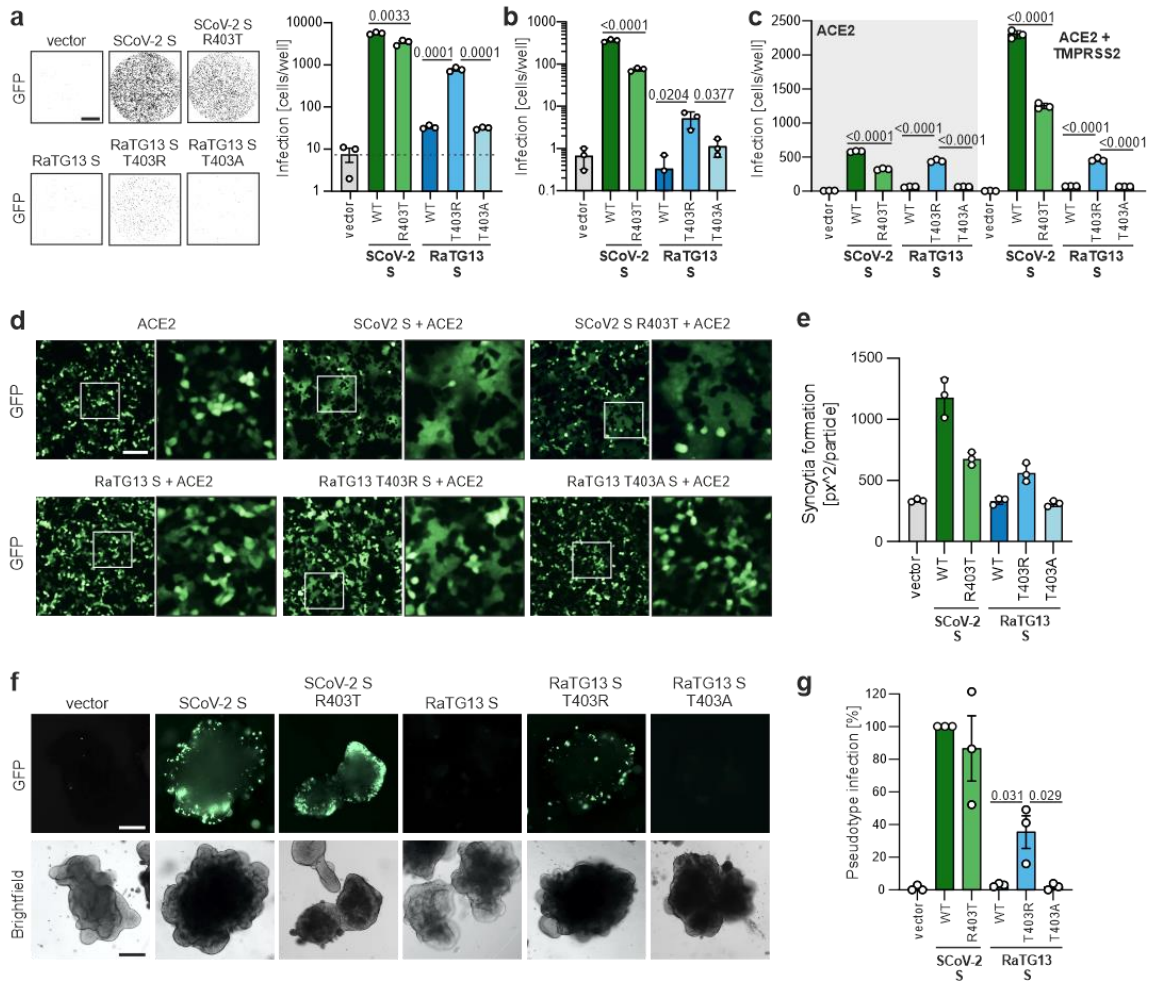

Figure 6: R403 in spike is crucial for ACE2-dependent entry. a, Binary images of CaCo-2 cells transduced with VSVΔG-GFP pseudotyped with SARS-CoV-2, RaTG13 or indicated mutant S. Successful infection events (=GFP positive cells) displayed as black dots. Scale bar, 1.5mm and automatic quantification of infection events by counting GFP positive cells. Bars represent the mean of three independent experiments (±SEM). **b,** Automatic quantification of infection events of Calu-3 cells transduced with VSVΔG-GFP pseudotyped with SARS-CoV-2, RaTG13 or indicated mutant S. Bars represent the mean of three independent experiments (±SEM). **c,** Automatic quantification of infection events of A549 ACE2 and A549 ACE2 and TMPRSS2 expressing cells transduced with VSVΔG-GFP pseudotyped with SARS-CoV-2, RaTG13 or indicated mutant S. Bars represent the mean of three independent experiments (±SEM). **d,** fluorescence microscopy images of HEK293T cells expressing SARS-CoV-2 S, RaTG13 S or the indicated mutant, Human ACE2 and GFP (green). Insets are indicated by white boxes. Scale bar, 125µm. The images represent a single experiment. **e,** Automated size quantification of the syncytia represented in (d). Bars represent the mean of three independent experiments (±SEM).**f,** Bright field and fluorescence microscopy (GFP) images of hPSC derived gut organoids, cultured and provided by A.H. were infected with VSVΔG-GFP (green) pseudotyped with SARS-CoV-2, RaTG13 or indicated mutant S (300 µl, 2 h). Scale bar, 250µm and quantification of the percentage of GFP-positive cells of (f). Bars represent the mean of three independent experiments (±SEM) From Zech et al., 2021 CC BY 4.0

To confirm the enhancing effect of T403R observed in the PP system with a SARS-CoV-2 backbone, SARS-CoV-2 lacking the S ORF (SARS-CoV-2ΔS, replicon System) was complimented with WT or R403T mutant SARS-CoV-2 S in ACE2-expressing HEK293T cells, which in both cases led to visible virus-induced cytopathic effects (CPE) (Fig. 7a). Unlike complementation with WT or T403A RaTG13, the T403R RaTG13 S resulted in significant CPE, which correlated with Gaussia luciferase (GLuc) expression signal (Fig. 7b). To further asses the relevance of R403 for SARS-CoV-2 replication, bacmids specifically containing the R403T mutation and coding for the yellow fluorescent protein (YFP) in place of ORF6 were utilized to rescue a replication-competent SARS-CoV-2. R403T S was efficiently expressed and incorporated into viral particles, albeit at slightly reduced levels compared to the WT SARS-CoV-2 S (Supplementary Fig. 3). Replication monitoring of the rescued SARS-CoV-2 R403T in Caco-2 cells after initial infection with a low MOI of 0.005 showed significantly lower efficiency than the WT virus (Fig. 7c). Thus, data obtained with replication-competent SARS-CoV-2 confirmed the results of S-mediated VSVpp infection and the replicon assays.

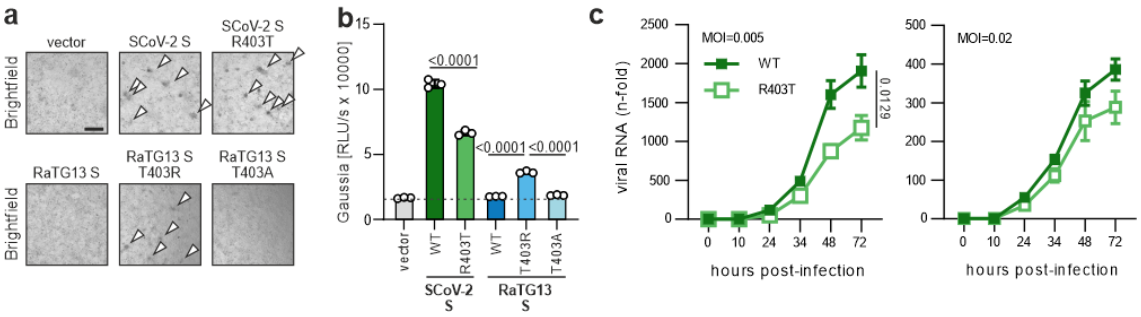

Figure 7: R403 in spike is relevant for replication-competent SARS-CoV--2 a, Bright field microscopy of HEK293T cells transfected with SARS-CoV-2ΔS bacmid, SARS-CoV-2-N, ACE2, T7 polymerase and indicated S variants. Scale bar, 125µm. Arrows indicate syncytia. **b,** Quantification of Gaussia luciferase activity in the supernatant of HEK293T cells expressing SARS-CoV-2ΔS-Gaussia bacmids as described in (a). Bars represent the mean of three independent experiments (±SEM). **c,** Replication kinetic of Caco-2 cells, infected with either SARS-CoV-2 d6-YFP wild type or SARS-CoV-2 d6-YFP R403T (MOI 0.005 or 0.02). Supernatants were collected at the indicated time points post-infection, and replication was determined by RT-qPCR. Lines represent the mean of three independent experiments (±SEM). A.H. and A.C. performed the rescue and replication monitoring of WT SARS-CoV-2 and R403T mutat virus. From Zech et al., 2021 CC BY 4.0

3.4 The enhancing effect of T403R depends on E37 in ACE2.

REAXX based computational analyses suggest that R403 promotes S-mediated infection of human cells because of electrostatic interaction of E37 in human ACE2 (Fig. 5c). To further

investigate the role of R403 during ACE2 binding, E37 was mutated in ACE2 to Alanine, removing the negative charge. Western blot confirmed stable expression levels of the ACE2 mutants (Fig. 8a). HEK293T cells were transfected with the ACE2 mutants and infected with VSVΔG-eGFP pseudotyped with parental and 403 mutant S proteins. Infection of SARS-CoV-2 WT and R403T VSVpp converge, when E37 was mutated. In agreement with the *in silico* prediction, T403R RaTG13 S VSVpp lost their advantage when E37 in ACE2 was mutated. Mutation of the proximal and also negatively charged D38 only reduced R403T VSVpp infection by 20%, and WT SARS-CoV-2 kept its advantage over the R403T mutated S (Fig. 8b). The increased ability of S R403 to bind human ACE2, was further confirmed by an in vitro S/ACE2 interaction assay. HEK293T cells were transfected with S-V5 and lysed. Half of the lysate was transferred in ACE2 coated plates (Fig. 8c) and incubated. S protein still binding ACE2 after washing is detected by an αV5-Ms and quantified using a secondary HRP-conjugated anti-mouse Ab. The remaining lysate was utilized to determine S-V5 expression. Albeit SARS-CoV-2 S was expressed at lower levels compared to the RaTG13 S (Fig. 8d) it bound efficiently to human ACE2 (Fig. 8e). R403T in SARS-CoV-2 S reduced the levels of S protein bound to ACE2, an effect that may be partly due to reduced S expression levels. However, the T403R substitution in RaTG13 S strongly enhanced levels of S protein bound to ACE2 without affecting RaTG13 S expression levels (Fig. 8e).

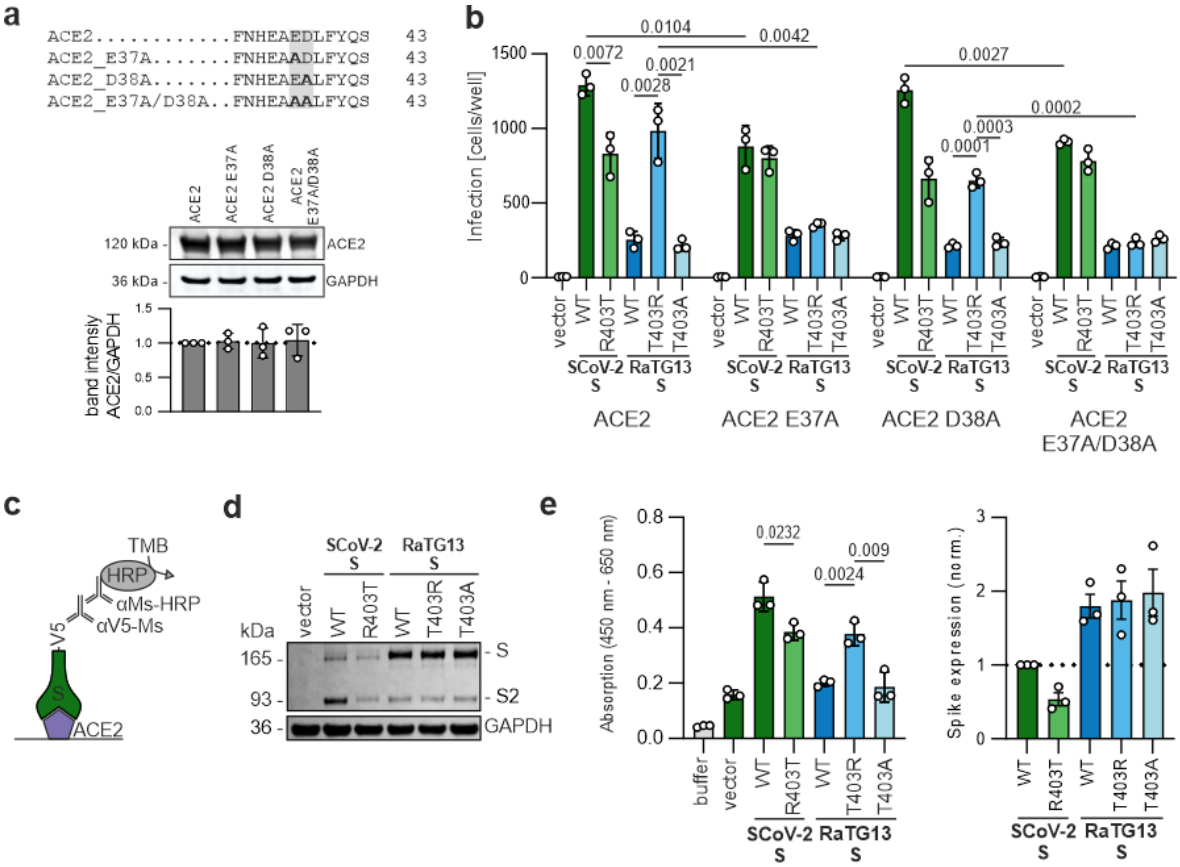

Figure 8: The enhancing effect of T403R in RaTG13 S depends on E37 in ACE2. a, Mutations introduced into human ACE2 (upper) and exemplary immunoblot of whole cells lysates (WCLs) of HEK293T cells expressing the indicated ACE2 constructs. Blots were stained with anti-ACE2 and anti-GAPDH and quantified for ACE2 expression (lower panel). Bars represent the mean of three independent experiments (±SEM). **b,** HEK293T cells expressing indicated ACE2 constructs were infected with VSVΔG-GFP pseudotyped with SARS-CoV-2, RaTG13 or indicated mutant S. Quantification by automatic counting of GFP positive cells. Bars represent the mean of three independent experiments (±SEM) **c,** Schematic representation of the ACE2 interaction assay. **d,** Exemplary immunoblots of WCLs of HEK293T cells expressing SARS-CoV-2 S, RaTG13 S or the indicated mutant. Blots were stained with anti-SARS-CoV-2 S, anti-GAPDH and quantified for S expression. **e,** ACE2 binding using whole cell lysates of HEK293T expressing SARS-CoV-2, RaTG13 or indicated mutant S. Bars represent the mean of three independent experiments (±SEM). From Zech et al., 2021 CC BY 4.0

3.5 RaTG13 S T403R increases ACE2-dependent proteolytic processing.

Coronavirus entry critically depends on the proteolytic processing of the S protein (Hoffmann & Pöhlmann, 2021a). Sequential cleavage of SARS-CoV-2 S first by furin at the S1/S2 site and subsequently by TMPRSS2 or Cathepsin B/L at the S2` site is required for efficient infection. RaTG13 S lacks the poly-basic furin cleavage site, which contributes to the high infectivity of SARS-CoV-2, while the presumed TMPRSS2 cleavage site is conserved (Fig. 9a).

Expression and incorporation of the WT and mutant S proteins into the VSVΔG particles was confirmed by western blot analyses (Fig. 9b). As expected, processing at the S1/S2 site was less efficient for RaTG13 than for SARS-CoV-2 S, as RATG13 S lacks the highly efficient Furin cleavage side. (Fig. 9b). Interaction of the S protein with its human receptor ACE2 promotes TMPRSS2/Cathepsin B/L dependant proteolytic processing of the S2' side. Indeed, ACE2 coexpression induced processing of the WT and R403T SARS-CoV-2 as well as T403R RaTG13 S2 proteins to the fusogenic S2` subunit. Cleavage of the WT and T403A RaTG13 S proteins remained inefficient (Fig. 9b).

RaTG13 T403R S VSVpp infection of A549 is TMPRSS2 independent (Fig. 6c). It has been reported that the cysteine proteases Cathepsin B/L can activate S in the absence of TMPRSS2. Indeed, the Cathepsin inhibitor E64-d, but not the TMPRSS2 inhibitor Camostat, prevented SARS-CoV-2 and T403R RaTG13 S-mediated VSVpp infection of ACE2-A549 cells (Fig. 9c). Thus, Cathepsins mediate activation of S2 to S2` during RaTG13 T403R-dependent infection of ACE2-A549 cells.

R403 generates a potential RGD integrin-binding motive, which might also be present in SARS-CoV-2 S (Fig. 4a). However, the integrin inhibitor ATN-161 had no effect on SARS-CoV-2 or T403R RaTG13 S-mediated infection of Caco-2 cells, nor on infection of Calu-3 cells with a Clade 19A WT SARS-CoV-2 isolate (Fig. 9d).

Further, cell-cell fusion in the presence of specific inhibitors was examined. Furin-inhibitor-1 prevented and the Cathepsin inhibitor E64-d moderately reduced SARS-CoV-2 and RaTG13 T403R S-mediated syncytia formation (Fig. 9e**)**. In contrast, the TMPRSS2 inhibitor Camostat had little if any effect on the S-mediated cell fusion. Altogether, mutation of T403R allows RaTG13 S interaction with human ACE2 and proteolytic activation by furin and Cathepsins for both cell-cell fusion and RaTG13 S-mediated VSVpp entry.

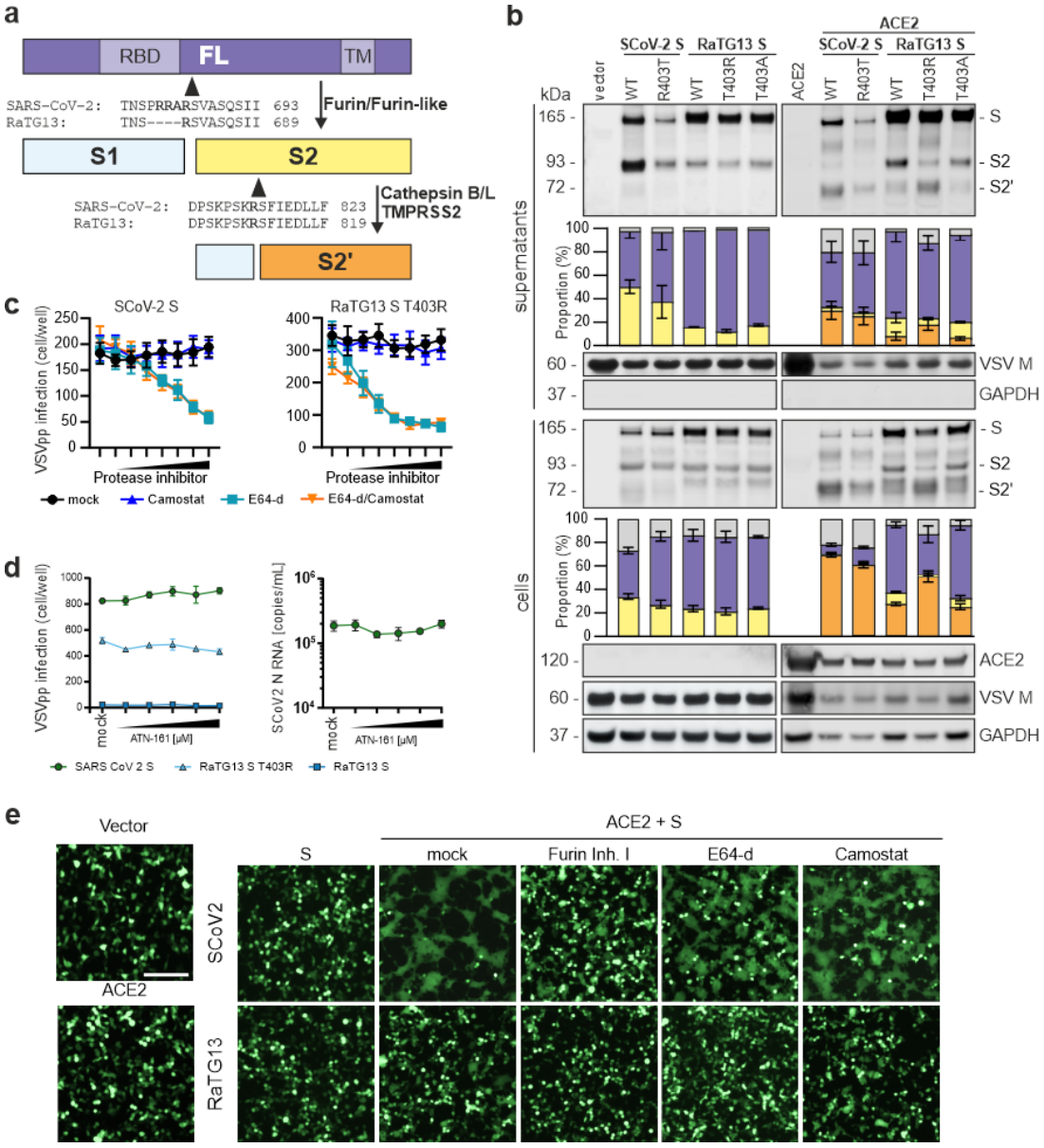

Figure 9: Interaction with ACE2 enhances S processing. a, Schematic representation of the SARS-CoV-2 S protein and sequence alignments of the SARS-CoV-2 and RaTG13 S1/S2 and S2' cleavage sites. **b,** Exemplary immunoblots of whole cells lysates (WCLs) and supernatants of HEK293T cells expressing SARS-CoV-2 S, RaTG13 S or the indicated mutant that were infected with VSVΔG-GFP in the absence (left) or the presence of a vector expressing human ACE2 (right). Blots were stained with anti-SARS-CoV-2 S, anti-GAPDH, anti-ACE2 and anti-VSV-M. and quantified for S FL, S2 and S2' expression. Bars represent the mean of three independent experiments (±SEM). **c,** Automated quantification of GFP fluorescence of A549 ACE2 cells infected with VSVΔG-GFP pseudotyped with indicated SARS-CoV-2 or RaTG13 S in the absence of ACE2. The cells were pre-treated (30 min) with 20 µM of E64d or Camostat in the highest concentration and further diluted in a 1:2 titration. Lines represent the mean of three independent experiments (±SEM). **d,** Automated quantification by GFP fluorescence of Caco-2 cells preincubated with indicated amounts of α5β5 integrin Inhibitor ATN-161 and infected with VSVΔG-GFP pseudotyped with SARS-CoV-2, RaTG13 T403R mutant or RaTG13 S. Lines represent the mean of three independent experiments (±SEM) and quantification of viral RNA copies in the supernatant of Calu-3 cells preincubated with indicated amounts of ATN-161 and

infected SARS-CoV-2 (MOI 0.05, 6 h). Lines represent the mean of three independent experiments (±SEM). **e,** Exemplary fluorescence microscopy images of HEK293T cells expressing SARS-CoV-2 S or RaTG13 S, Human ACE2 and GFP (green). The cells were incubated with the indicated protease inhibitor. Scale bar, 125µm. From Zech et al., 2021 CC BY 4.0

3.6 The ability of T403R RaTG13 S to utilize ACE2 is species-specific.

To examine whether SARS-CoV-2 and RaTG13 S can utilize bat ACE2 for cell entry, we overexpressed human and bat-derived ACE2 in HEK293T cells and examined their susceptibility to S-mediated VSVpp infection. As expected, the WT SARS-CoV-2 and the T403R RaTG13 S proteins efficiently infected HEK293T cells overexpressing human ACE2, while the parental RaTG13 S protein was poorly active (Fig. 10a). The original RaTG13 sequence was isolated from dropping of *Rhinolophus affinis*. Thus, it came as surprise that RaTG13 S was hardly able to use *Rhinolophus affinis* derived ACE2 for infection (Fig. 10a). The WT RaTG13 S protein used *R. pusillus* ACE2 with very poor efficiency und was unable to use *R. macrotis* ACE2 for infection, suggesting that RaTG13 might use an alternative receptor for infection of bat cells.

To validate the results obtained with human HEK293T cells, we utilized the lung epithelial cell line Tb1 Lu1 of *Tadarida brasiliensis*. As this cell line lacks endogenous ACE2 expression, it did not support infection by CoV S proteins (Fig. 10b). Engineered expression of human ACE2, however, made Lu 1 cells highly susceptible to infection mediated by SARS-CoV-2 and the T403R RaTG13 S proteins (Fig. 10b). Entry mediated by R403T SARS-CoV-2 S was strongly attenuated and the WT and T403A RaTG13 S proteins were unable to mediate VSV-pp infection.

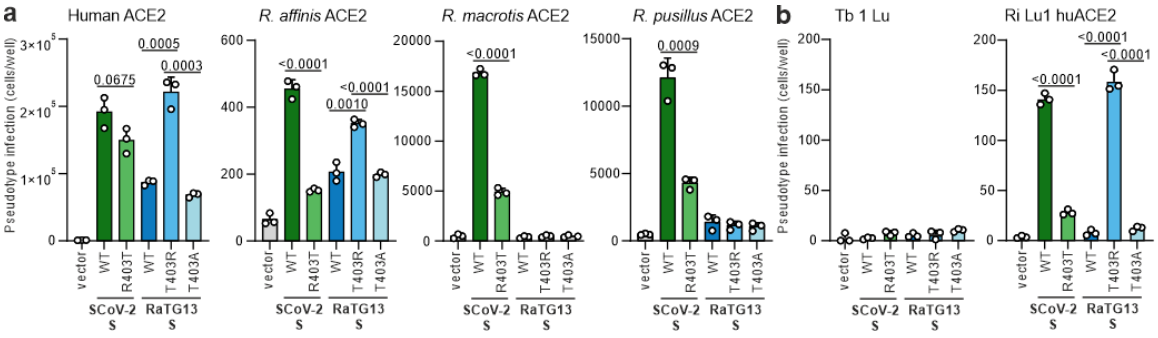

Figure 10: SARS-CoV-2 S and T403R RaTG13 S allow entry with human but not bat ACE2. a, HEK293T cells expressing indicated ACE2 variants or **b,** Tb 1 Lu, *Tadarida brasiliensis* derived lung epithelial and Ri 1 Lu huACE2 *Rhinolophus affinis* derived lung epithelial cells expressing human ACE2 were infected with VSVΔG-GFP pseudotyped with SARS-CoV-2, RaTG13 or indicated mutant S. Quantification by automatic counting of GFP positive cells. Bars represent the mean of three independent experiments (±SEM). From Zech et al., 2021 CC BY 4.0

3.7 COVID-19 vaccination cross-neutralizes SARS-CoV-1 spike and enhances inhibition of hCoV-OC43 spike-mediated infection

The S proteins of the SARS-related CoV share 76% sequence identity, and it was previously reported that serum of COVID-19 vaccinated individuals can cross-neutralize the SARS-CoV-1 S protein (Grobben et al., 2021). To further investigate if sera from COVID-19 vaccinated individuals also neutralize the S protein of other human CoVs, we collected sera of six individuals directly before and two weeks after the second BNT162b2 vaccination. The collected sera was titered against VSV- or HIV-based pseudo particles containing the S proteins of SARS-CoV-1, SARS-CoV-2, MERS-CoV and hCoV-OC43, -NL63 and -229E (Fig 11a). While COVID-19 immunization induced immunity against SARS-CoV-2 S mediated infection (Fig. 11b), the sera of COVID-19 vaccinated individuals also inhibited infection mediated by SARS-CoV-1, but not the MERS-CoV S. COVID19 vaccination further enhanced a strong preexisting humoral immunity against pseudovirions carrying the hCoV-OC43 S protein (Fig 11b). At the same time, there was no enhancing effect of the immunity against NL63 or 229E S mediated infection (Fig 11b).

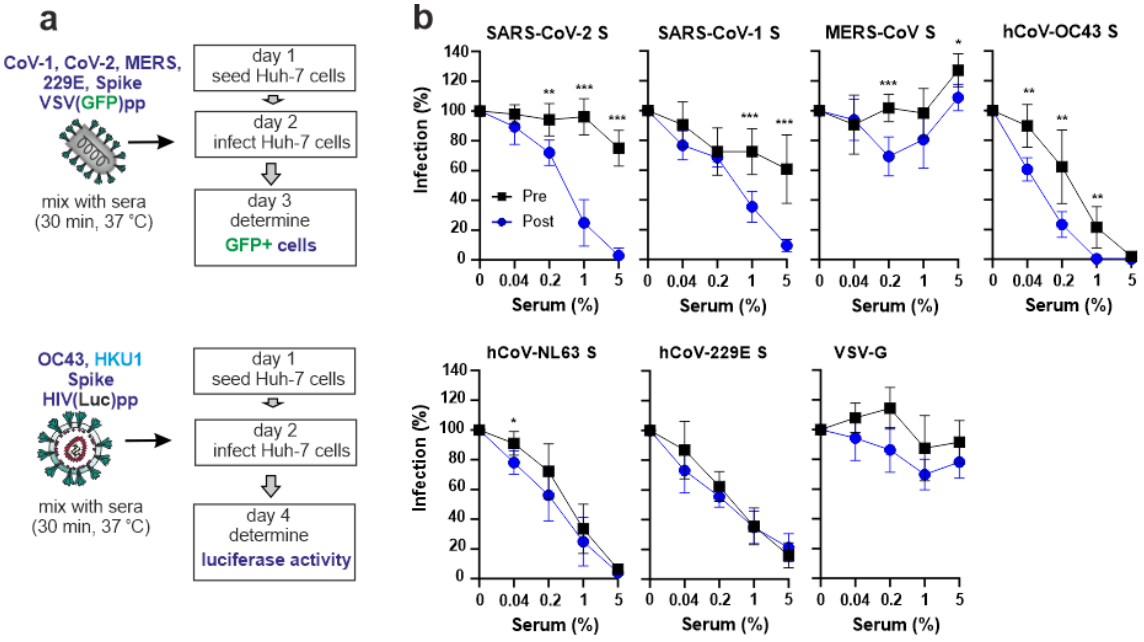

Figure 11: Neutralization of pseudoparticles containing the spike-proteins of highly pathogenic or circulating seasonal CoVs. a, Schematic presentation of S-mediated VSVpp or HIVpp infection. **b,** Neutralization of VSVpp or HIVpp containing the indicated S proteins or the VSV-G for control by sera obtained before(Pre) and after (Post) vaccination compared to the untreated control (100%). Shown are mean values (±SEM; n=6). From Lawrenz et al., 2022 CC BY-NC-ND 4.0

3.8 RaTG13 S T403R is sensitive to sera from vaccinated individuals.

The increased infectiousness of the T403R RaTG13 S enabled us to examine its sensitivity to therapeutic agents and serum neutralization. EK-1 is a fusion inhibitor with reported broad panCoV activity (Xia et al., 2019). As expected, EK-1 efficiently inhibited SARS-CoV-2 and T403R RaTG13 S mediated fusion. Pangolin-CoV S mediated infection, however, was only slightly inhibited (Fig. 12a). The highly specific monoclonal antibody Casirivirab was only active against SARS-CoV-2 S (Fig. 12b). However, sera from three COVID-19 vaccinated individuals, collected two weeks after their second vaccination with the BNT162b2 vaccine, neutralized T403R RaTG13 S with higher efficiency than the SARS-CoV-2 S (Fig. 12c). To further analyze the sensitivity of the T403R RaTG13 S to vaccine-induced serum neutralization, we examined sera from 22 individuals vaccinated heterologously with the ChAdOx1 nCoV-19/BNT162b2 vaccine and further nine individuals who received homologous BNT162b2 vaccination. As the more efficient neutralization of RaTG13 S in the initial experiments might be biased by the high infection rate of SARS-COV-2 S particles, VSVpp stocks were normalized for the same infectivity (Fig. 12c). All sera inhibited RaTG13 T403R S-mediated infection, albeit with varying efficiencies (Fig. 12d). On average, sera obtained after heterologous and homologous vaccination regimens showed similar neutralization efficiencies against RaTG13 T403R (Fig. 12e) and SARS-CoV-2 (Fig. 12f).

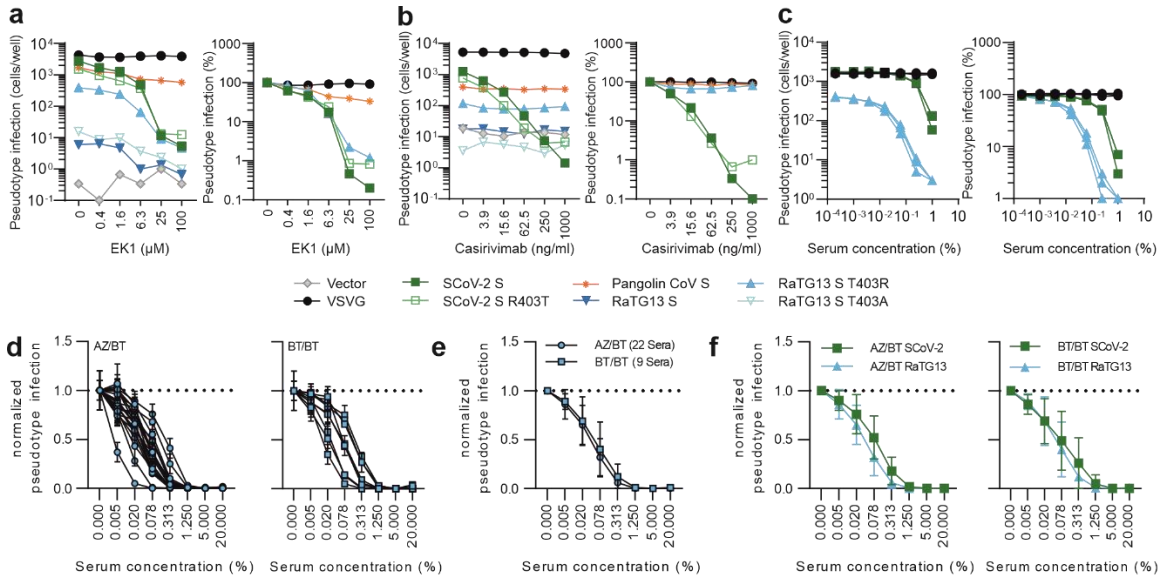

Figure 12: T403R RaTG13 S is sensitive to EK-1 and sera from vaccinated individuals but not Casivirimab. a-c, Automated quantification of GFP fluorescence of Caco-2 cells infected with VSVΔG-GFP pseudotyped with indicated S variants. The virus was pre-treated (30 min) with the indicated amounts of **a,**

EK-1 **b,** Casirivimab **(**orange**),** and **c,** Sera of BNT162b2 vaccinated patients. Lines represent the mean of three independent experiments (±SEM). **d,** Sera of AZ/BNT162b2 and 2xBNT162b2 vaccinated patients with VSVΔG-GFP pseudotyped with RaTG13 S. Lines represent the mean of three biological replicates. **e, f,** Mean of the inhibition of VSVΔG-GFP pseudotyped with **e,** RaTG13 S by Sera of AZ/BNT162b2 or 2x BNT162b2 vaccinated patients and **f,** RaTG13 S or SARS-CoV-2 by the Sera of AZ/BNT162b2 (left) or 2x BNT162b2 (right) vaccinated patients. Lines represent the mean of three independent experiments (±SEM). From Zech et al., 2021 CC BY 4.0

4. Discussion

Bats and pangolins across Southeast Asia carry viruses with high sequence similarity to the first sampled SARS-COV-2 sequences. The bat coronavirus RaTG13 shares 96% sequence identity with SARS-CoV-2, which made RaTG13 the closest bat relative of SARS-CoV-2 during the initiation of my thesis (Ge et al., 2013; P. Zhou et al., 2020a).

Initial infection experiments revealed low infectiousness of RaTG13 S pseudo particles, which, considering the high sequence similarity to SARS-CoV-2, came as surprise (Fig. 4b). REAX-based molecular modeling, together with a rational approach, allowed us to determine position 403 as a major difference between the S proteins of Sarbecoviruses, which efficiently utilize human ACE2 and RaTG13 S (Fig. 5a). The involvement of a positive charge at S position 403 in binding human ACE2 by establishing electrostatic interaction with E37 was described before (Laurini et al., 2020, 2021; Lim et al., 2020; Williams & Zhan, 2021). R403 is positioned 30 amino acids upstream of the defined SARS-CoV-2 receptor binding motif (Lan et al., 2020). However, REAX based molecular modeling confirmed that the Arginine side-chain of R403 reaches into the binding interface between SARS-CoV-2 S and ACE2, where it establishes putative charge interactions to the negatively charged ACE2 E37 (Fig. 5b). Numerous residues in the SARS-CoV-2 S RBD are involved in the interaction with the human ACE2 receptor (Shang et al., 2020). Thus, R403T substitution in the SARS-CoV-2 S only moderately reduced VSV pseudo particle infection. In contrast, site-directed mutagenesis of RaTG13 S T403R led to a ~30-fold increase of pseudoparticle infectivity of human lung- and intestine-derived cell lines as well as hPSC-derived gut organoids and drastically enhanced syncytia formation after ACE2/S cotransfection (Fig. 6) making T403R a requirement of RaTG13 S to mediate efficient ACE2-dependent infection. A recent study proposed that residue 501 beneath others in the RBM plays a key role in the ability of RaTG13 S to use human ACE2 (K. Liu, Pan, et al., 2021b). Those changes allowed the RaTG13 S protein to infect human cells almost as efficiently as the SARS-CoV-2 S.

REAX based molecular modeling suggested E37 in ACE2 as the main interaction partner of SARS-CoV-2 S 403R. Indeed, mutation of E37 in ACE2 reduced WT SARS-CoV-2 S-mediated infection levels to those obtained for the R403T SARS-CoV-2 S (Fig. 8b), suggesting that the interaction between R403 in the S protein and E37 in the ACE2 receptor is relevant for full infectiousness of SARS-CoV-2. However, reduced expression levels and incorporation of the R403T mutant SARS-CoV-2 S also seem to contribute. Strikingly, the

complete loss of the T403R mediated increased ACE2 binding experimentally confirmed E37 as the primary interaction partner of RaTG13 S 403R during ACE2 binding. Some individuals show rare polymorphisms of E37K introducing a positive charge at ACE2 position 37 (frequency: 3.27e-5; gnomAD, https://gnomad.broadinstitute.org), which was reported to impair S binding. It is tempting to speculate that these individuals might have a reduced risk for infection and/or severe COVID-19.

The change of 403R completes an RGD motif in the sequence of RaTG13. For several viruses, such as Adeno Associated- or Hanta-virus, RGD-dependent Integrin binding and thus increased infection have been described (Gavrilovskaya et al., 1998; Summerford et al., 1999). If the SARS-CoV-2 RGD is accessible to $\alpha_5\beta_1$ Integrin, thereby increasing host cell interaction, remains under debate (Beaudoin et al., 2021; Makowski et al., 2021; Othman et al., 2022) and, while there was no significant effect of the $\alpha_5\beta_1$ integrin-binding peptide ANT-161 on SARS-CoV-2 and RaTG13 T403R as well as WT SARS-CoV-2 (Supplementary Fig.5), a possible role of the RGD motif for the interaction with other integrins cannot be excluded entirely but remains speculative.

The glycoproteins of many enveloped viruses are activated by proteolytic cleavage. SARS-CoV-2 S depends on furin-like mediated cleavage during glycoprotein synthesis and CathepsinL/TMPRSS2 processing to liberate the N-terminal fusion peptide of the S2' subunit (Jackson et al., 2022). In agreement with published data, SARS-CoV-2 S binding of ACE2 strongly enhanced proteolytic processing of SARS-CoV-2 S into its fusogenic S2' subunit (Raghuvamsi et al., 2021). Similarly, cotransfection of ACE2 increased the processing of RaTG13 T403R S (Fig. 9b), further underlining the importance of R403 for efficient ACE2 binding and subsequent membrane fusion.

RaTG13 S lacks the polybasic insertion at the S1/S2 site, which promotes furin-mediated processing of SARS-CoV-2 S (Hoffmann, Kleine-Weber, & Pöhlmann, 2020; F. Li, 2016). Thus, it was expected that the efficiency of proteolytic processing of RaTG13 S proteins at the S1/S2 site is reduced (Fig. 9b). It was unexpected, however, that overexpression of TMPRSS2 only enhanced VSVpp infection mediated by the SARS-CoV-2 but not by the RaTG13 T403R S protein (Fig. 9b) since the S2`cleavage site that is targeted by TMPRSS2 is identical in these S proteins. Instead, processing of the RaTG13 S at the S2' site was dependent on Cathepsins, which have also been shown to efficiently cleave the SARS-CoV-2 S in some cell types (Zhao et al., 2021), thus suggesting a primarily endosomal driven entry for RaTG13. This possibility is further supported by the inhibition of T403R RaTG13

by the Cathepsin B/L inhibitor E64d (Fig. 9c). While Cathepsin L dependency of SARS-CoV-2 had been described before, the exclusive dependency of a closely related SARS-CoV-2 precursor on endosomal driven entry suggests that SARS-CoV-2 acquired cell membrane fusion somewhen before or during its adaption to humans.

SARS-CoV-2 is a zoonotic virus and SARS-CoV-2-related bat viruses with sequence identity above 90 % have been sampled from bats all across southeast Asia (Fig. 2) (Delaune et al., 2021; Mallapaty, 2021; Temmam et al., 2021; H. Zhou et al., 2021). Bat Sarbecoviruses that are less related to SARS-CoV-2 but can use the human ACE2 receptor, were identified in Japan and eastern Russia (Murakami et al., 2020; Seifert & Letko, 2021). It has been shown that the RBD of SARS-CoV-2 S shows higher homology to the corresponding region of the pangolin CoV S protein or the recently discovered BANAL-20-52 isolate from *Rhinolophus malayanus* in Laos than to RaTG13 (Lam et al., 2020b; Temmam et al., 2021; Xiao et al., 2021). Whether or not this is a consequence of recombination or convergent evolution is under debate. Notably, both BANAL-20-52 and Pan CoV S protein contain a positively charged residue at position 403 and can utilize human ACE2 for infection (Fig. 5d, e). BANAL-20-52 is a closer relative to SARS-CoV-2 than RaTG13, indicating that a change in residue 403 may have occurred before the emergence of SARS-CoV-2. Altogether our results suggest that a positively charged amino acid residue at position 403 in the S protein was a prerequisite for efficient zoonotic transmission and pandemic spread of SARS-CoV-2. Notably, a positively charged residue at the corresponding position is present in S proteins of most RaTG13-related bat coronaviruses (Fig. 5d,e). Thus, many bat Sarbecoviruses, including the unknown precursor of SARS-CoV-2, may be fitter for zoonotic transmission than RaTG13.

The cellular receptor of RaTG13 in bats is unknown (K. Liu, Pan, et al., 2021b). To further investigate whether RaTG13 is able to utilize bat-derived ACE2, we infected HEK293T cells expressing the Human, *R. affiensis*, *R. macrotis* and *R. pussillus* ACE2. While SARS-COV-2 was able to utilize the ACE2 of all listed bat species, RaTG13 S laking the T403R mutation was hardly able to utilize human and *R. affiensis* ACE2, and not able to use the ACE2 of *R. macrotis* and *R. pusillus* for infection. RaTG13 was isolated from droppings of *R. affinis*, consistent with that, WT RaTG13 can utilize *R. affinis* ACE2 as a cellular receptor, albeit with lower efficiency than human ACE2. Further research is needed on the receptor usage of Sarbecoviruses in their host organisms and a potential dependency on alternative receptors. This is further underlined by the fact that neither SASR-CoV-2, nor RaTG13 was

able to infect the bat-derived lung cell line Tb 1 Lu and artificial expression of Human ACE2 is a prerequisite for infection of the bat-derived lung cell line Ri Lu 1 (Fig. 10b).

Sera of individuals fully vaccinated with the BNT162b2 vaccine cross neutralized SARS-CoV-1 S almost as efficient as the S protein of SARS-CoV-2 (Fig. 11b). Cross neutralization of the SARS Coronaviruses was previously observed and is explained by the high sequence similarity of the viral S proteins (Dangi et al., 2021). There was no increased neutralization against MERS-CoV S mediated infection after COVID-19 vaccination. All six tested sera showed preexisting humoral immunity against CoVs OC43, NL63 and 229E (Fig. 11b). Neutralisation of NL63 and 229E S before and after vaccination remained similar. However, the neutralizing activity against OC43 S increased significantly two weeks after boost vaccination. One previous study did not observe differences in the antibody titers against seasonal coronaviruses after SARS-CoV-2 infection (Iyer et al., 2020). Our results, however, agree with results showing that SARS-CoV-2 infection induces neutralizing antibodies against SARS-CoV-1 and hCoV-OC43 and that sera from humans who received SARS-CoV-2 vaccines exert protective effects against various coronaviruses in mice (Aydillo et al., 2021; Dangi et al., 2021; Kaplonek et al., 2021; Secchi et al., 2020). In support of a protective role, it has been documented that recent infection with common cold coronaviruses (CCC) is associated with less severe COVID-19 (Galipeau et al., 2021) and while the increase in immunity is certainly not driven by CCC neutralizing titers, high CCC-specific CD4+ T cell reactivity is associated with pre-existing SARS-CoV-2 immunity (Yu et al., 2022). However, strong cross-protection between CCC and SARS-CoV-2 after COVID-19 vaccination seems unlikely. The induced neutralisation was usually modest and common cold viruses cause repeated infections despite preexisting immunity (Sagar et al., 2021). The increase in infectivity of T403R RaTG13 VSV pseudoparticles enabeled us to determine inhibition and neutralisation of RaTG13 S by antiviral compounds and sera of COVID-19 vaccinated individuals. The pan-CoV fusion inhibitor EK-1 was reported to inhibit MERS, SARS, 229E, NL63, and OC43 CoV S proteins as well as the bat SARS-like RS3367 and WIV-1 CoV S protein (Fig. 12a) with IC50s in the low µM range (Xia et al., 2019). Thus, it was not surprising that RaTG13 T403R S-driven entry was blocked by EK-1. Pangolin CoV S, however, was only slightly inhibited by EK-1. In contrast, Casirivimab, a monoclonal antibody approved for COVID-19 therapy in the US and Europe, had no activity against RaTG13 T403R S. Epitope binding of neutralizing antibodies is often impaired by a single amino acid change and especially the monotherapeutic use of such

highly specific antibodies will foster fast escape by mutations. A fact that was impressively demonstrated by the recent emergence of the Omicron SARS-CoV-2 variant and it being resistant to a vast majority of the clinically approved monoclonal antibodies (Iketani et al., 2022; Mellott et al., 2021; Pastorio et al., 2022). However, RaTG13 and SARS-COV-2 were similarly neutralised by sera of 2x Biontech (BNT162b2) or AZ/BT vaccinated individuals, thus indicating that those first-generation vaccines also protect against animal counterparts of SARS-CoV 2. The SARS-CoV-2 omicron VOC and RaTG13 S share 96.2 % and 96.7 % of its sequence with the original Hu-1 S. However, SARS-CoV-2 omicron almost completely evades serum-mediated neutralization after immunisation with vaccines based on the original Hu-1 sequence (Pastorio et al., 2022). While adapted SARS-COV-2 vaccines are currently in clinical trials (https://www.pfizer.com/news) immunisation with first-generation COVID-19 vaccines might still be a valuable tool to avoid future zoonotic events with Sarbecoviruses.

5. Summary

While sharing over 96% sequence identity with SARS-CoV-2 S, the RaTG13 S protein poorly binds human ACE2. However, a single amino acid change of T403R allowed RaTG13 S to efficiently utilize human ACE2 for viral entry. REAX based molecular modeling confirmed that the Arginin side-chain of R403 reaches into the binding interface between SARS-CoV-2 S and ACE2, allowing putative charge interaction to the negatively charged ACE2 E37. Mutation of E37A not only abolished the enhancing effect of the T403R change on RaTG13 S-mediated VSVpp infection but also reduced infection mediated by the SARS-CoV-2 S. Similarly to SARS-COV-2, cotransfection of ACE2 lead to Cathepsin dependent processing of RaTG13 T403R S into its fusogenic S2' subunit, suggesting a primarily endosomal driven and TEMPRSS2 independent entry for RaTG13. A positively charged residue at S position 403 is present in most RaTG13-related bat coronaviruses, suggesting that many bat Sarbecoviruses, including the unknown precursor of SARS-CoV-2, are fitter for zoonotic transmission than RaTG13.

Sera of individuals fully vaccinated with the BNT162b2 vaccine cross neutralized SARS-CoV-1 S almost as efficient as the S protein of SARS-CoV-2. Neutralizing activity against the S protein of the seasonal Coronavirus OC43 increased significantly two weeks after boost vaccination. Ultimately, the increased infectiousness of T403R RaTG13 S enabled us to examine its sensitivity to serum of AZ/BT or BT/BT COVID-19 vaccinated individuals. The efficient neutralisation of RaTG13 S by those sera indicates that first-generation vaccines also protect against animal counterparts of SARS-CoV 2 that may emerge in the future

Bibliography

Alagaili, A. N., Briese, T., Mishra, N., Kapoor, V., Sameroff, S. C., de Wit, E., Munster, V. J., Hensley, L. E., Zalmout, I. S., Kapoor, A., Epstein, J. H., Karesh, W. B., Daszak, P., Mohammed, O. B., & lan Lipkin, W. (2014). Middle east respiratory syndrome coronavirus infection in dromedary camels in Saudi Arabia. *MBio*, *5*(2). https://doi.org/10.1128/mBio.00884-14

Alharbi, N. K., Qasim, I., Almasoud, A., Aljami, H. A., Alenazi, M. W., Alhafufi, A., Aldibasi, O. S., Hashem, A. M., Kasem, S., Albrahim, R., Aldubaib, M., Almansour, A., Temperton, N. J., Kupke, A., Becker, S., Abu-obaidah, A., Alkarar, A., Yoon, I. K., Azhar, E., … Balkhy, H. H. (2019). Humoral Immunogenicity and Efficacy of a Single Dose of ChAdOx1 MERS Vaccine Candidate in Dromedary Camels. *Scientific Reports 2019 9:1*, *9*(1), 1–11. https://doi.org/10.1038/s41598-019-52730-4

Aydillo, T., Rombauts, A., Stadlbauer, D., Aslam, S., Abelenda-Alonso, G., Escalera, A., Amanat, F., Jiang, K., Krammer, F., Carratala, J., & García-Sastre, A. (2021). Immunological imprinting of the antibody response in COVID-19 patients. *Nature Communications*, *12*(1), 1–13. https://doi.org/10.1038/s41467-021-23977-1

Baden, L. R., El Sahly, H. M., Essink, B., Kotloff, K., Frey, S., Novak, R., Diemert, D., Spector, S. A., Rouphael, N., Creech, C. B., McGettigan, J., Khetan, S., Segall, N., Solis, J., Brosz, A., Fierro, C., Schwartz, H., Neuzil, K., Corey, L., … Zaks, T. (2021). Efficacy and Safety of the mRNA-1273 SARS-CoV-2 Vaccine. *New England Journal of Medicine*, *384*(5), 403–416. https://doi.org/10.1056/nejmoa2035389

Baum, A., Fulton, B. O., Wloga, E., Copin, R., Pascal, K. E., Russo, V., Giordano, S., Lanza, K., Negron, N., Ni, M., Wei, Y., Atwal, G. S., Murphy, A. J., Stahl, N., Yancopoulos, G. D., & Kyratsous, C. A. (2020). Antibody cocktail to SARS-CoV-2 spike protein prevents rapid mutational escape seen with individual antibodies. *Science*, *369*(6506), 1014–1018. https://doi.org/10.1126/science.abd0831

Beaudoin, C. A., Hamaia, S. W., Huang, C. L. H., Blundell, T. L., & Jackson, A. P. (2021). Can the SARS-CoV-2 Spike Protein Bind Integrins Independent of the RGD Sequence? *Frontiers in Cellular and Infection Microbiology*, *11*, 1116. https://doi.org/10.3389/fcimb.2021.765300

Bestle, D., Heindl, M. R., Limburg, H., van Lam van, T., Pilgram, O., Moulton, H., Stein, D. A., Hardes, K., Eickmann, M., Dolnik, O., Rohde, C., Klenk, H. D., Garten, W., Steinmetzer, T., & Böttcher-Friebertshäuser, E. (2020). TMPRSS2 and furin are both essential for proteolytic activation of SARS-CoV-2 in human airway cells. *Life Science Alliance*, *3*(9). https://doi.org/10.26508/LSA.202000786

Carlson, C. J., Albery, G. F., Merow, C., Trisos, C. H., Zipfel, C. M., Eskew, E. A., Olival, K. J., Ross, N., & Bansal, S. (2022). Climate change increases cross-species viral transmission risk. *Nature*. https://doi.org/10.1038/S41586-022-04788-W

Chakraborty, H., Tarafdar, P. K., Klapper, D. G., & Lentz, B. R. (2013). Wild-type and mutant hemagglutinin fusion peptides alter bilayer structure as well as kinetics and activation thermodynamics of stalk and pore formation differently: Mechanistic implications. *Biophysical Journal*, *105*(11), 2495–2506. https://doi.org/10.1016/j.bpj.2013.10.010

Chu, D. K. W., Leung, C. Y. H., Gilbert, M., Joyner, P. H., Ng, E. M., Tse, T. M., Guan, Y., Peiris, J. S. M., & Poon, L. L. M. (2011). Avian Coronavirus in Wild Aquatic Birds.

Journal of Virology, *85*(23), 12815–12820. https://doi.org/10.1128/jvi.05838-11

Corman, V. M., Muth, D., Niemeyer, D., & Drosten, C. (2018a). Hosts and Sources of Endemic Human Coronaviruses. *Advances in Virus Research*, *100*, 163–188. https://doi.org/10.1016/BS.AIVIR.2018.01.001

Corman, V. M., Muth, D., Niemeyer, D., & Drosten, C. (2018b). Hosts and Sources of Endemic Human Coronaviruses. In *Advances in Virus Research* (Vol. 100, pp. 163–188). Elsevier. https://doi.org/10.1016/bs.aivir.2018.01.001

Dangi, T., Palacio, N., Sanchez, S., Park, M., Class, J., Visvabharathy, L., Ciucci, T., Koralnik, I. J., Richner, J. M., & Penaloza-MacMaster, P. (2021). Cross-protective immunity following coronavirus vaccination and coronavirus infection. *Journal of Clinical Investigation*, *131*(24). https://doi.org/10.1172/JCI151969

Delaune, D., Hul, V., Karlsson, E. A., Hassanin, A., Ou, T. P., Baidaliuk, A., Gámbaro, F., Prot, M., Tu, V. T., Chea, S., Keatts, L., Mazet, J., Johnson, C. K., Buchy, P., Dussart, P., Goldstein, T., Simon-Lorière, E., & Duong, V. (2021). A novel SARS-CoV-2 related coronavirus in bats from Cambodia. *Nature Communications*, *12*(1), 2021.01.26.428212. https://doi.org/10.1038/s41467-021-26809-4

Desai, D., Khan, A. R., Soneja, M., Mittal, A., Naik, S., Kodan, P., Mandal, A., Maher, G. T., Kumar, R., Agarwal, A., Gowda, N. R., H, V., Kumar, P., Pandey, S., Pandey, R. M., Kumar, A., Ray, A., Jorwal, P., Nischal, N., … Guleria, R. (2022). Effectiveness of an inactivated virus-based SARS-CoV-2 vaccine, BBV152, in India: a test-negative, case-control study. *The Lancet Infectious Diseases*, *22*(3), 349–356. https://doi.org/10.1016/S1473-3099(21)00674-5

Ding, Y., He, L., Zhang, Q., Huang, Z., Che, X., Hou, J., Wang, H., Shen, H., Qiu, L., Li, Z., Geng, J., Cai, J., Han, H., Li, X., Kang, W., Weng, D., Liang, P., & Jiang, S. (2004). Organ distribution of severe acute respiratory syndrome (SARS) associated coronavirus (SARS-CoV) in SARS patients: Implications for pathogenesis virus transmission pathways. *Journal of Pathology*, *203*(2), 622–630. https://doi.org/10.1002/path.1560

Falsey, A. R., Sobieszczyk, M. E., Hirsch, I., Sproule, S., Robb, M. L., Corey, L., Neuzil, K. M., Hahn, W., Hunt, J., Mulligan, M. J., McEvoy, C., DeJesus, E., Hassman, M., Little, S. J., Pahud, B. A., Durbin, A., Pickrell, P., Daar, E. S., Bush, L., … Gonzalez-Lopez, A. (2021). Phase 3 Safety and Efficacy of AZD1222 (ChAdOx1 nCoV-19) Covid-19 Vaccine. *New England Journal of Medicine*, *385*(25), 2348–2360. https://doi.org/10.1056/nejmoa2105290

Faria, N. R., Rambaut, A., Suchard, M. A., Baele, G., Bedford, T., Ward, M. J., Tatem, A. J., Sousa, J. D., Arinaminpathy, N., Pépin, J., Posada, D., Peeters, M., Pybus, O. G., & Lemey, P. (2014). The early spread and epidemic ignition of HIV-1 in human populations. *Science*, *346*(6205), 56–61. https://doi.org/10.1126/science.1256739

Forni, D., Cagliani, R., Arrigoni, F., Benvenuti, M., Mozzi, A., Pozzoli, U., Clerici, M., de Gioia, L., & Sironi, M. (2021). Adaptation of the endemic coronaviruses HCoV-OC43 and HCoV-229E to the human host. *Virus Evolution*, *7*(2). https://doi.org/10.1093/ve/veab061

Galipeau, Y., Siragam, V., Laroche, G., Marion, E., Greig, M., McGuinty, M., Booth, R. A., Durocher, Y., Cuperlovic-Culf, M., Bennett, S. A. L., Crawley, A. M., Giguère, P. M., Cooper, C., & Langlois, M. A. (2021). Relative Ratios of Human Seasonal Coronavirus Antibodies Predict the Efficiency of Cross-Neutralization of SARS-CoV-2 Spike

Binding to ACE2. *EBioMedicine*, *74*, 103700. https://doi.org/10.1016/J.EBIOM.2021.103700/ATTACHMENT/B3BA9C16-8C09-4560-8EB9-BF1FDB3B978A/MMC3.XLSX

Gavrilovskaya, I. N., Shepley, M., Shaw, R., Ginsberg, M. H., & Mackow, E. R. (1998). B3 Integrins Mediate the Cellular Entry of Hantaviruses That Cause Respiratory Failure. *Proceedings of the National Academy of Sciences of the United States of America*, *95*(12), 7074–7079. https://doi.org/10.1073/pnas.95.12.7074

Ge, X. Y., Li, J. L., Yang, X. Lou, Chmura, A. A., Zhu, G., Epstein, J. H., Mazet, J. K., Hu, B., Zhang, W., Peng, C., Zhang, Y. J., Luo, C. M., Tan, B., Wang, N., Zhu, Y., Crameri, G., Zhang, S. Y., Wang, L. F., Daszak, P., & Shi, Z. L. (2013). Isolation and characterization of a bat SARS-like coronavirus that uses the ACE2 receptor. *Nature*, *503*(7477), 535–538. https://doi.org/10.1038/nature12711

Ge, X. Y., Wang, N., Zhang, W., Hu, B., Li, B., Zhang, Y. Z., Zhou, J. H., Luo, C. M., Yang, X. Lou, Wu, L. J., Wang, B., Zhang, Y., Li, Z. X., & Shi, Z. L. (2016). Coexistence of multiple coronaviruses in several bat colonies in an abandoned mineshaft. *Virologica Sinica*, *31*(1), 31–40. https://doi.org/10.1007/s12250-016-3713-9

Gharbharan, A., Jordans, C. C. E., GeurtsvanKessel, C., den Hollander, J. G., Karim, F., Mollema, F. P. N., Stalenhoef – Schukken, J. E., Dofferhoff, A., Ludwig, I., Koster, A., Hassing, R. J., Bos, J. C., van Pottelberge, G. R., Vlasveld, I. N., Ammerlaan, H. S. M., van Leeuwen – Segarceanu, E. M., Miedema, J., van der Eerden, M., Schrama, T. J., … Rijnders, B. J. A. (2021). Effects of potent neutralizing antibodies from convalescent plasma in patients hospitalized for severe SARS-CoV-2 infection. *Nature Communications*, *12*(1), 1–12. https://doi.org/10.1038/s41467-021-23469-2

Grobben, M., Van Der Straten, K., Brouwer, P. J., Brinkkemper, M., Maisonnasse, P., Dereuddre-Bosquet, N., Appelman, B., Ayesha Lavell, A. H., Van Vught, L. A., Burger, J. A., Poniman, M., Oomen, M., Eggink, D., Bijl, T. P., Van Willigen, H. D., Wynberg, E., Verkaik, B. J., Figaroa, O. J., De Vries, P. J., … Van Gils, M. J. (2021). Cross-reactive antibodies after sars-cov-2 infection and vaccination. *ELife*, *10*, 1–20. https://doi.org/10.7554/eLife.70330

Haagmans, B. L., Al Dhahiry, S. H. S., Reusken, C. B. E. M., Raj, V. S., Galiano, M., Myers, R., Godeke, G. J., Jonges, M., Farag, E., Diab, A., Ghobashy, H., Alhajri, F., Al-Thani, M., Al-Marri, S. A., Al Romaihi, H. E., Al Khal, A., Bermingham, A., Osterhaus, A. D. M. E., AlHajri, M. M., & Koopmans, M. P. G. (2014). Middle East respiratory syndrome coronavirus in dromedary camels: An outbreak investigation. *The Lancet Infectious Diseases*, *14*(2), 140–145. https://doi.org/10.1016/S1473-3099(13)70690-X

Heath, P. T., Galiza, E. P., Baxter, D. N., Boffito, M., Browne, D., Burns, F., Chadwick, D. R., Clark, R., Cosgrove, C., Galloway, J., Goodman, A. L., Heer, A., Higham, A., Iyengar, S., Jamal, A., Jeanes, C., Kalra, P. A., Kyriakidou, C., McAuley, D. F., … Toback, S. (2021). Safety and Efficacy of NVX-CoV2373 Covid-19 Vaccine. *New England Journal of Medicine*, *385*(13), 1172–1183. https://doi.org/10.1056/nejmoa2107659

Hoffmann, M., Arora, P., Groß, R., Seidel, A., Hörnich, B. F., Hahn, A. S., Krüger, N., Graichen, L., Hofmann-Winkler, H., Kempf, A., Winkler, M. S., Schulz, S., Jäck, H. M., Jahrsdörfer, B., Schrezenmeier, H., Müller, M., Kleger, A., Münch, J., & Pöhlmann, S. (2021). SARS-CoV-2 variants B.1.351 and P.1 escape from neutralizing antibodies. *Cell*, *184*(9), 2384-2393.e12. https://doi.org/10.1016/j.cell.2021.03.036

Hoffmann, M., Kleine-Weber, H., & Pöhlmann, S. (2020). A Multibasic Cleavage Site in the Spike Protein of SARS-CoV-2 Is Essential for Infection of Human Lung Cells. *Molecular Cell*, *78*(4), 779-784.e5. https://doi.org/10.1016/j.molcel.2020.04.022

Hoffmann, M., Kleine-Weber, H., Schroeder, S., Krüger, N., Herrler, T., Erichsen, S., Schiergens, T. S., Herrler, G., Wu, N. H., Nitsche, A., Müller, M. A., Drosten, C., & Pöhlmann, S. (2020a). SARS-CoV-2 Cell Entry Depends on ACE2 and TMPRSS2 and Is Blocked by a Clinically Proven Protease Inhibitor. *Cell*, *181*(2), 271-280.e8. https://doi.org/10.1016/j.cell.2020.02.052

Hoffmann, M., Kleine-Weber, H., Schroeder, S., Krüger, N., Herrler, T., Erichsen, S., Schiergens, T. S., Herrler, G., Wu, N. H., Nitsche, A., Müller, M. A., Drosten, C., & Pöhlmann, S. (2020b). SARS-CoV-2 Cell Entry Depends on ACE2 and TMPRSS2 and Is Blocked by a Clinically Proven Protease Inhibitor. *Cell*, *181*(2), 271-280.e8. https://doi.org/10.1016/j.cell.2020.02.052

Hoffmann, M., & Pöhlmann, S. (2021a). How SARS-CoV-2 makes the cut. *Nature Microbiology*, *6*(7), 828–829. https://doi.org/10.1038/s41564-021-00931-x

Hoffmann, M., & Pöhlmann, S. (2021b). How SARS-CoV-2 makes the cut. *Nature Microbiology*, *6*(7), 828–829. https://doi.org/10.1038/s41564-021-00931-x

Huang, Y., Yang, C., Xu, X. feng, Xu, W., & Liu, S. wen. (2020). Structural and functional properties of SARS-CoV-2 spike protein: potential antivirus drug development for COVID-19. *Acta Pharmacologica Sinica*, *41*(9), 1141–1149. https://doi.org/10.1038/s41401-020-0485-4

Iketani, S., Liu, L., Guo, Y., Liu, L., Chan, J. F. W., Huang, Y., Wang, M., Luo, Y., Yu, J., Chu, H., Chik, K. K. H., Yuen, T. T. T., Yin, M. T., Sobieszczyk, M. E., Huang, Y., Yuen, K. Y., Wang, H. H., Sheng, Z., & Ho, D. D. (2022). Antibody evasion properties of SARS-CoV-2 Omicron sublineages. *Nature 2022 604:7906*, *604*(7906), 553–556. https://doi.org/10.1038/s41586-022-04594-4

Iyer, A. S., Jones, F. K., Nodoushani, A., Kelly, M., Becker, M., Slater, D., Mills, R., Teng, E., Kamruzzaman, M., Garcia-Beltran, W. F., Astudillo, M., Yang, D., Miller, T. E., Oliver, E., Fischinger, S., Atyeo, C., Iafrate, A. J., Calderwood, S. B., Lauer, S. A., … Charles, R. C. (2020). Persistence and decay of human antibody responses to the receptor binding domain of SARS-CoV-2 spike protein in COVID-19 patients. *Science Immunology*, *5*(52). https://doi.org/10.1126/sciimmunol.abe0367

Jackson, C. B., Farzan, M., Chen, B., & Choe, H. (2022). Mechanisms of SARS-CoV-2 entry into cells. *Nature Reviews Molecular Cell Biology*, *23*(1), 3–20. https://doi.org/10.1038/s41580-021-00418-x

Jones, T. C., Biele, G., Mühlemann, B., Veith, T., Schneider, J., Beheim-Schwarzbach, J., Bleicker, T., Tesch, J., Schmidt, M. L., Sander, L. E., Kurth, F., Menzel, P., Schwarzer, R., Zuchowski, M., Hofmann, J., Krumbholz, A., Stein, A., Edelmann, A., Corman, V. M., & Drosten, C. (2021). Estimating infectiousness throughout SARS-CoV-2 infection course. *Science*, *373*(6551). https://doi.org/10.1126/science.abi5273

Jung, C., Kmiec, D., Koepke, L., Zech, F., Jacob, T., Sparrer, K. M. J., & Kirchhoff, F. (2022). Omicron: What Makes the Latest SARS-CoV-2 Variant of Concern So Concerning? *Journal of Virology*, *96*(6). https://doi.org/10.1128/jvi.02077-21

Kaplonek, P., Wang, C., Bartsch, Y., Fischinger, S., Gorman, M. J., Bowman, K., Kang, J., Dayal, D., Martin, P., Nowak, R. P., Villani, A. C., Hsieh, C. L., Charland, N. C.,

Gonye, A. L. K., Gushterova, I., Khanna, H. K., LaSalle, T. J., Lavin-Parsons, K. M., Lilley, B. M., … Alter, G. (2021). Early cross-coronavirus reactive signatures of humoral immunity against COVID-19. *Science Immunology*, *6*(64), 2901. https://doi.org/10.1126/sciimmunol.abj2901

Ke, Z., Oton, J., Qu, K., Cortese, M., Zila, V., McKeane, L., Nakane, T., Zivanov, J., Neufeldt, C. J., Cerikan, B., Lu, J. M., Peukes, J., Xiong, X., Kräusslich, H. G., Scheres, S. H. W., Bartenschlager, R., & Briggs, J. A. G. (2020). Structures and distributions of SARS-CoV-2 spike proteins on intact virions. *Nature*, *588*(7838), 498–502. https://doi.org/10.1038/s41586-020-2665-2

Krammer, F. (2020). SARS-CoV-2 vaccines in development. *Nature*, *586*(7830), 516–527. https://doi.org/10.1038/s41586-020-2798-3

Lam, T. T. Y., Jia, N., Zhang, Y. W., Shum, M. H. H., Jiang, J. F., Zhu, H. C., Tong, Y. G., Shi, Y. X., Ni, X. B., Liao, Y. S., Li, W. J., Jiang, B. G., Wei, W., Yuan, T. T., Zheng, K., Cui, X. M., Li, J., Pei, G. Q., Qiang, X., … Cao, W. C. (2020a). Identifying SARS-CoV-2-related coronaviruses in Malayan pangolins. *Nature*, *583*(7815), 282–285. https://doi.org/10.1038/s41586-020-2169-0

Lam, T. T. Y., Jia, N., Zhang, Y. W., Shum, M. H. H., Jiang, J. F., Zhu, H. C., Tong, Y. G., Shi, Y. X., Ni, X. B., Liao, Y. S., Li, W. J., Jiang, B. G., Wei, W., Yuan, T. T., Zheng, K., Cui, X. M., Li, J., Pei, G. Q., Qiang, X., … Cao, W. C. (2020b). Identifying SARS-CoV-2-related coronaviruses in Malayan pangolins. *Nature*, *583*(7815), 282–285. https://doi.org/10.1038/s41586-020-2169-0

Lan, J., Ge, J., Yu, J., Shan, S., Zhou, H., Fan, S., Zhang, Q., Shi, X., Wang, Q., Zhang, L., & Wang, X. (2020). Structure of the SARS-CoV-2 spike receptor-binding domain bound to the ACE2 receptor. *Nature*, *581*(7807), 215–220. https://doi.org/10.1038/s41586-020-2180-5

Lau, K. K., Yu, W. C., Chu, C. M., Lau, S. T., Sheng, B., & Yuen, K. Y. (2004). Possible Central Nervous System Infection by SARS Coronavirus. *Emerging Infectious Diseases*, *10*(2), 342–344. https://doi.org/10.3201/eid1002.030638

Laurini, E., Marson, D., Aulic, S., Fermeglia, A., & Pricl, S. (2021). Computational Mutagenesis at the SARS-CoV-2 Spike Protein/Angiotensin-Converting Enzyme 2 Binding Interface: Comparison with Experimental Evidence. *ACS Nano*, *15*(4), 6929–6948. https://doi.org/10.1021/acsnano.0c10833

Laurini, E., Marson, D., Aulic, S., Fermeglia, M., & Pricl, S. (2020). Computational Alanine Scanning and Structural Analysis of the SARS-CoV-2 Spike Protein/Angiotensin-Converting Enzyme 2 Complex. *ACS Nano*, *14*(9), 11821–11830. https://doi.org/10.1021/acsnano.0c04674

Lawrenz, J., Xie, Q., Zech, F., Weil, T., Seidel, A., Krnavek, D., van der Hoek, L., Münch, J., Müller, J. A., & Kirchhoff, F. (2022). Severe Acute Respiratory Syndrome Coronavirus 2 Vaccination Boosts Neutralizing Activity Against Seasonal Human Coronaviruses. *Clinical Infectious Diseases*, *75*(1), e653–e661. https://doi.org/10.1093/cid/ciac057

Leung, W. K., To, K., Chan, P. K. S., Chan, H. L. Y., Wu, A. K. L., Lee, N., Yuen, K. Y., & Sung, J. J. Y. (2003). Enteric involvement of severe acute respiratory syndrome-associated coronavirus infection. *Gastroenterology*, *125*(4), 1011–1017. https://doi.org/10.1016/s0016-5085(03)01215-0

Li, F. (2016). Structure, Function, and Evolution of Coronavirus Spike Proteins. *Annual Review of Virology*, *3*(1), 237–261. https://doi.org/10.1146/annurev-virology-110615-042301

Li, W., Moore, M. J., Vasllieva, N., Sui, J., Wong, S. K., Berne, M. A., Somasundaran, M., Sullivan, J. L., Luzuriaga, K., Greeneugh, T. C., Choe, H., & Farzan, M. (2003). Angiotensin-converting enzyme 2 is a functional receptor for the SARS coronavirus. *Nature*, *426*(6965), 450–454. https://doi.org/10.1038/nature02145

Li, W., Shi, Z., Yu, M., Ren, W., Smith, C., Epstein, J. H., Wang, H., Crameri, G., Hu, Z., Zhang, H., Zhang, J., McEachern, J., Field, H., Daszak, P., Eaton, B. T., Zhang, S., & Wang, L. F. (2005). Bats are natural reservoirs of SARS-like coronaviruses. *Science*, *310*(5748), 676–679. https://doi.org/10.1126/science.1118391

Lim, H., Baek, A., Kim, J., Kim, M. S., Liu, J., Nam, K. Y., Yoon, J. H., & No, K. T. (2020). Hot spot profiles of SARS-CoV-2 and human ACE2 receptor protein protein interaction obtained by density functional tight binding fragment molecular orbital method. *Scientific Reports*, *10*(1), 16862. https://doi.org/10.1038/s41598-020-73820-8

Liu, K., Ang, Pan, X., Li, L., Yu, F., Zheng, A., Du, P., Han, P., Meng, Y., Zhang, Y., Wu, L., Chen, Q., Song, C., Jia, Y., Niu, S., Lu, D., Qiao, C., Chen, Z., Ma, D., … Wang, Q. (2021). Binding and molecular basis of the bat coronavirus RaTG13 virus to ACE2 in humans and other species. *Cell*, *184*(13), 3438-3451.e10. https://doi.org/10.1016/j.cell.2021.05.031

Liu, K., Pan, X., Li, L., Yu, F., Zheng, A., Du, P., Han, P., Meng, Y., Zhang, Y., Wu, L., Chen, Q., Song, C., Jia, Y., Niu, S., Lu, D., Qiao, C., Chen, Z., Ma, D., Ma, X., … Wang, Q. (2021a). Binding and molecular basis of the bat coronavirus RaTG13 virus to ACE2 in humans and other species. *Cell*, *184*(13), 3438-3451.e10. https://doi.org/10.1016/j.cell.2021.05.031

Liu, K., Pan, X., Li, L., Yu, F., Zheng, A., Du, P., Han, P., Meng, Y., Zhang, Y., Wu, L., Chen, Q., Song, C., Jia, Y., Niu, S., Lu, D., Qiao, C., Chen, Z., Ma, D., Ma, X., … Wang, Q. (2021b). Binding and molecular basis of the bat coronavirus RaTG13 virus to ACE2 in humans and other species. *Cell*, *184*(13), 3438-3451.e10. https://doi.org/10.1016/j.cell.2021.05.031

Liu, P., Jiang, J. Z., Wan, X. F., Hua, Y., Li, L., Zhou, J., Wang, X., Hou, F., Chen, J., Zou, J., & Chen, J. (2020). Are pangolins the intermediate host of the 2019 novel coronavirus (SARS-CoV-2)? *PLoS Pathogens*, *16*(5), e1008421. https://doi.org/10.1371/journal.ppat.1008421

Logunov, D. Y., Dolzhikova, I. V., Shcheblyakov, D. V., Tukhvatulin, A. I., Zubkova, O. V., Dzharullaeva, A. S., Kovyrshina, A. V., Lubenets, N. L., Grousova, D. M., Erokhova, A. S., Botikov, A. G., Izhaeva, F. M., Popova, O., Ozharovskaya, T. A., Esmagambetov, I. B., Favorskaya, I. A., Zrelkin, D. I., Voronina, D. V., Shcherbinin, D. N., … Gintsburg, A. L. (2021). Safety and efficacy of an rAd26 and rAd5 vector-based heterologous prime-boost COVID-19 vaccine: an interim analysis of a randomised controlled phase 3 trial in Russia. *The Lancet*, *397*(10275), 671–681. https://doi.org/10.1016/S0140-6736(21)00234-8

Maki, J., Guiot, A. L., Aubert, M., Brochier, B., Cliquet, F., Hanlon, C. A., King, R., Oertli, E. H., Rupprecht, C. E., Schumacher, C., Slate, D., Yakobson, B., Wohlers, A., & Lankau, E. W. (2017). Oral vaccination of wildlife using a vaccinia-rabies-glycoprotein

recombinant virus vaccine (RABORAL V-RG®): A global review. *Veterinary Research*, *48*(1), 1–26. https://doi.org/10.1186/s13567-017-0459-9

Makowski, L., Olson-Sidford, W., & Weisel, J. W. (2021). Biological and clinical consequences of integrin binding via a rogue rgd motif in the sars cov-2 spike protein. *Viruses*, *13*(2), 146. https://doi.org/10.3390/v13020146

Mallapaty, S. (2021). Closest known relatives of virus behind COVID-19 found in Laos. *Nature*, *597*(7878), 603. https://doi.org/10.1038/d41586-021-02596-2

Mathieu, E., Ritchie, H., Ortiz-Ospina, E., Roser, M., Hasell, J., Appel, C., Giattino, C., & Rodés-Guirao, L. (2021). A global database of COVID-19 vaccinations. *Nature Human Behaviour*, *5*(7), 947–953. https://doi.org/10.1038/s41562-021-01122-8

Medicine, L. S. of H. and T. (2021). *COVID-19 Vaccine Tracker*. COVID-19 Vaccne Tracker. https://vac-lshtm.shinyapps.io/ncov_vaccine_landscape/

Mellott, D. M., Tseng, C. Te, Drelich, A., Fajtová, P., Chenna, B. C., Kostomiris, D. H., Hsu, J., Zhu, J., Taylor, Z. W., Kocurek, K. I., Tat, V., Katzfuss, A., Li, L., Giardini, M. A., Skinner, D., Hirata, K., Yoon, M. C., Beck, S., Carlin, A. F., … McKerrow, J. H. (2021). A Clinical-Stage Cysteine Protease Inhibitor blocks SARS-CoV-2 Infection of Human and Monkey Cells. *ACS Chemical Biology*, *16*(4), 642–650. https://doi.org/10.1021/ACSCHEMBIO.0C00875/SUPPL_FILE/CB0C00875_SI_001.PDF

Murakami, S., Kitamura, T., Suzuki, J., Sato, R., Aoi, T., Fujii, M., Matsugo, H., Kamiki, H., Ishida, H., Takenaka-Uema, A., Shimojima, M., & Horimoto, T. (2020). Detection and Characterization of Bat Sarbecovirus Phylogenetically Related to SARS-CoV-2, Japan. *Emerging Infectious Diseases*, *26*(12), 3025–3029. https://doi.org/10.3201/eid2612.203386

O'Driscoll, M., Ribeiro Dos Santos, G., Wang, L., Cummings, D. A. T., Azman, A. S., Paireau, J., Fontanet, A., Cauchemez, S., & Salje, H. (2021). Age-specific mortality and immunity patterns of SARS-CoV-2. *Nature*, *590*(7844), 140–145. https://doi.org/10.1038/s41586-020-2918-0

Othman, H., Messaoud, H. Ben, Khamessi, O., Ben-Mabrouk, H., Ghedira, K., Bharuthram, A., Treurnicht, F., Achilonu, I., Sayed, Y., & Srairi-Abid, N. (2022). SARS-CoV-2 Spike Protein Unlikely to Bind to Integrins via the Arg-Gly-Asp (RGD) Motif of the Receptor Binding Domain: Evidence From Structural Analysis and Microscale Accelerated Molecular Dynamics. *Frontiers in Molecular Biosciences*, *9*, 60. https://doi.org/10.3389/fmolb.2022.834857

Palacios, R., Patiño, E. G., de Oliveira Piorelli, R., Conde, M. T. R. P., Batista, A. P., Zeng, G., Xin, Q., Kallas, E. G., Flores, J., Ockenhouse, C. F., & Gast, C. (2020). Double-Blind, Randomized, Placebo-Controlled Phase III Clinical Trial to Evaluate the Efficacy and Safety of treating Healthcare Professionals with the Adsorbed COVID-19 (Inactivated) Vaccine Manufactured by Sinovac – PROFISCOV: A structured summary of a . *Trials*, *21*(1), 853. https://doi.org/10.1186/s13063-020-04775-4

Pastorio, C., Zech, F., Noettger, S., Jung, C., Jacob, T., Sparrer, K. M. J., & Kirchhoff, F. (2022). Determinants of Spike Infectivity, Processing and Neutralization in SARS-CoV-2 Omicron subvariants BA.1 and BA.2. *BioRxiv*, 2022.04.13.488221. https://doi.org/10.1101/2022.04.13.488221

Peacock, T. P., Goldhill, D. H., Zhou, J., Baillon, L., Frise, R., Swann, O. C., Kugathasan,

R., Penn, R., Brown, J. C., Sanchez-David, R. Y., Braga, L., Williamson, M. K., Hassard, J. A., Staller, E., Hanley, B., Osborn, M., Giacca, M., Davidson, A. D., Matthews, D. A., & Barclay, W. S. (2021). The furin cleavage site in the SARS-CoV-2 spike protein is required for transmission in ferrets. *Nature Microbiology*, *6*(7), 899–909. https://doi.org/10.1038/s41564-021-00908-w

Plante, J. A., Liu, Y., Liu, J., Xia, H., Johnson, B. A., Lokugamage, K. G., Zhang, X., Muruato, A. E., Zou, J., Fontes-Garfias, C. R., Mirchandani, D., Scharton, D., Bilello, J. P., Ku, Z., An, Z., Kalveram, B., Freiberg, A. N., Menachery, V. D., Xie, X., … Shi, P. Y. (2021). Spike mutation D614G alters SARS-CoV-2 fitness. *Nature*, *592*(7852), 116–121. https://doi.org/10.1038/s41586-020-2895-3

Polack, F. P., Thomas, S. J., Kitchin, N., Absalon, J., Gurtman, A., Lockhart, S., Perez, J. L., Pérez Marc, G., Moreira, E. D., Zerbini, C., Bailey, R., Swanson, K. A., Roychoudhury, S., Koury, K., Li, P., Kalina, W. V., Cooper, D., Frenck, R. W., Hammitt, L. L., … Gruber, W. C. (2020). Safety and Efficacy of the BNT162b2 mRNA Covid-19 Vaccine. *New England Journal of Medicine*, *383*(27), 2603–2615. https://doi.org/10.1056/nejmoa2034577

Raghuvamsi, P. V., Tulsian, N. K., Samsudin, F., Qian, X., Purushotorman, K., Yue, G., Kozma, M. M., Hwa, W. Y., Lescar, J., Bond, P. J., Macary, P. A., & Anand, G. S. (2021). Sars-cov-2 s protein:Ace2 interaction reveals novel allosteric targets. *ELife*, *10*, 1–47. https://doi.org/10.7554/eLife.63646

Ramadan, N., & Shaib, H. (2019). Middle east respiratory syndrome coronavirus (MERS-COV): A review. *Germs*, *9*(1), 35–42. https://doi.org/10.18683/germs.2019.1155

Saey, T. H. (2013). Story one: Scientists race to understand deadly new virus: SARS-like infection causes severe illness, but may not spread quickly among people. *Science News*, *183*(6), 5–6. https://doi.org/10.1002/scin.5591830603

Sagar, M., Reifler, K., Rossi, M., Miller, N. S., Sinha, P., White, L. F., & Mizgerd, J. P. (2021). Recent endemic coronavirus infection is associated with less-severe COVID-19. *Journal of Clinical Investigation*, *131*(1). https://doi.org/10.1172/JCI143380

Saito, A., Irie, T., Suzuki, R., Maemura, T., Nasser, H., Uriu, K., Kosugi, Y., Shirakawa, K., Sadamasu, K., Kimura, I., Ito, J., Wu, J., Iwatsuki-Horimoto, K., Ito, M., Yamayoshi, S., Loeber, S., Tsuda, M., Wang, L., Ozono, S., … Sato, K. (2021). Enhanced fusogenicity and pathogenicity of SARS-CoV-2 Delta P681R mutation. *Nature*, *22*(11), 1–7. https://doi.org/10.1038/s41586-021-04266-9

Secchi, M., Bazzigaluppi, E., Brigatti, C., Marzinotto, I., Tresoldi, C., Rovere-Querini, P., Poli, A., Castagna, A., Scarlatti, G., Zangrillo, A., Ciceri, F., Piemonti, L., & Lampasona, V. (2020). COVID-19 survival associates with the immunoglobulin response to the SARS-cov-2 spike receptor binding domain. *Journal of Clinical Investigation*, *130*(12), 6366–6378. https://doi.org/10.1172/JCI142804

Seifert, S. N., & Letko, M. C. (2021). A sarbecovirus found in Russian bats uses human ACE2 (preprint). *BioRxiv*, *December 7, 2021*, 1–14. https://doi.org/10.1101/2021.12.05.471310

Shang, J., Ye, G., Shi, K., Wan, Y., Luo, C., Aihara, H., Geng, Q., Auerbach, A., & Li, F. (2020). Structural basis of receptor recognition by SARS-CoV-2. *Nature*, *581*(7807), 221–224. https://doi.org/10.1038/s41586-020-2179-y

Sharp, P. M., & Hahn, B. H. (2011). Origins of HIV and the AIDS pandemic. *Cold Spring*

Harbor Perspectives in Medicine, *1*(1), a006841. https://doi.org/10.1101/cshperspect.a006841

Skowronski, D. M., Astell, C., Brunham, R. C., Low, D. E., Petric, M., Roper, R. L., Talbot, P. J., Tam, T., & Babiuk, L. (2005). Severe acute respiratory syndrome (SARS): A year in review. *Annual Review of Medicine*, *56*, 357–381. https://doi.org/10.1146/annurev.med.56.091103.134135

Song, H. D., Tu, C. C., Zhang, G. W., Wang, S. Y., Zheng, K., Lei, L. C., Chen, Q. X., Gao, Y. W., Zhou, H. Q., Xiang, H., Zheng, H. J., Chern, S. W. W., Cheng, F., Pan, C. M., Xuan, H., Chen, S. J., Luo, H. M., Zhou, D. H., Liu, Y. F., … Zhao, G. P. (2005). Cross-host evolution of severe acute respiratory syndrome coronavirus in palm civet and human. *Proceedings of the National Academy of Sciences of the United States of America*, *102*(7), 2430–2435. https://doi.org/10.1073/pnas.0409608102

Summerford, C., Bartlett, J. S., & Samulski, R. J. (1999). αVβ5 integrin: A co-receptor for adeno-associated virus type 2 infection. *Nature Medicine*, *5*(1), 78–82. https://doi.org/10.1038/4768

Taylor, L. H., Latham, S. M., & Woolhouse, M. E. J. (2001). Risk factors for human disease emergence. *Philosophical Transactions of the Royal Society B: Biological Sciences*, *356*(1411), 983–989. https://doi.org/10.1098/rstb.2001.0888

Temmam, S., Vongphayloth, K., Baquero, E., Munier, S., Bonomi, M., Regnault, B., Douangboubpha, B., Karami, Y., Chrétien, D., Sanamxay, D., Xayaphet, V., Paphaphanh, P., Lacoste, V., Somlor, S., Lakeomany, K., Phommavanh, N., Pérot, P., Dehan, O., Amara, F., … Eloit, M. (2022). Bat coronaviruses related to SARS-CoV-2 and infectious for human cells. *Nature*, *604*(7905), 330–336. https://doi.org/10.1038/s41586-022-04532-4

Temmam, S., Vongphayloth, K., Salazar, E. B., Munier, S., Bonomi, M., Régnault, B., Douangboubpha, B., Karami, Y., Chretien, D., Sanamxay, D., Xayaphet, V., Paphaphanh, P., Lacoste, V., Somlor, S., Lakeomany, K., Phommavanh, N., Pérot, P., Donati, F., Bigot, T., … Eloit, M. (2021). Coronaviruses with a SARS-CoV-2-like receptor- binding domain allowing ACE2-mediated entry into human cells isolated from bats of Indochinese peninsula. *Research Square*, *September 17th*. https://doi.org/10.21203/RS.3.RS-871965/V1

V'kovski, P., Kratzel, A., Steiner, S., Stalder, H., & Thiel, V. (2021). Coronavirus biology and replication: implications for SARS-CoV-2. *Nature Reviews Microbiology*, *19*(3), 155–170. https://doi.org/10.1038/s41579-020-00468-6

Wacharapluesadee, S., Tan, C. W., Maneeorn, P., Duengkae, P., Zhu, F., Joyjinda, Y., Kaewpom, T., Chia, W. N., Ampoot, W., Lim, B. L., Worachotsueptrakun, K., Chen, V. C. W., Sirichan, N., Ruchisrisarod, C., Rodpan, A., Noradechanon, K., Phaichana, T., Jantarat, N., Thongnumchaima, B., … Wang, L. F. (2021). Evidence for SARS-CoV-2 related coronaviruses circulating in bats and pangolins in Southeast Asia. *Nature Communications*, *12*(1), 972. https://doi.org/10.1038/s41467-021-21240-1

Walls, A. C., Park, Y. J., Tortorici, M. A., Wall, A., McGuire, A. T., & Veesler, D. (2020a). Structure, Function, and Antigenicity of the SARS-CoV-2 Spike Glycoprotein. *Cell*, *181*(2), 281-292.e6. https://doi.org/10.1016/j.cell.2020.02.058

Walls, A. C., Park, Y. J., Tortorici, M. A., Wall, A., McGuire, A. T., & Veesler, D. (2020b). Structure, Function, and Antigenicity of the SARS-CoV-2 Spike Glycoprotein. *Cell*,

181(2), 281-292.e6. https://doi.org/10.1016/j.cell.2020.02.058

Wang, L. F., & Eaton, B. T. (2007). Bats, civets and the emergence of SARS. *Current Topics in Microbiology and Immunology*, *315*, 325–344. https://doi.org/10.1007/978-3-540-70962-6_13

Wang, N., Luo, C., Liu, H., Yang, X., Hu, B., Zhang, W., Li, B., Zhu, Y., Zhu, G., Shen, X., Peng, C., & Shi, Z. (2019). Characterization of a new member of alphacoronavirus with unique genomic features in rhinolophus bats. *Viruses*, *11*(4), 379. https://doi.org/10.3390/v11040379

Williams, A. H., & Zhan, C. G. (2021). Fast prediction of binding affinities of the sars-cov-2 spike protein mutant n501y (UK variant) with ace2 and miniprotein drug candidates. *Journal of Physical Chemistry B*, *125*(17), 4330–4336. https://doi.org/10.1021/acs.jpcb.1c00869

World Health Organization. (2003). *Epidemic and Pandemic Alert Response: Summary of probable SARS cases with onset of illness from 1 November 2002 to 31 July 2003*. Based Data. https://www.who.int/publications/m/item/summary-of-probable-sars-cases-with-onset-of-illness-from-1-november-2002-to-31-july-2003

Wrobel, A. G., Benton, D. J., Xu, P., Roustan, C., Martin, S. R., Rosenthal, P. B., Skehel, J. J., & Gamblin, S. J. (2020). SARS-CoV-2 and bat RaTG13 spike glycoprotein structures inform on virus evolution and furin-cleavage effects. *Nature Structural and Molecular Biology*, *27*(8), 763–767. https://doi.org/10.1038/s41594-020-0468-7

Wu, F., Zhao, S., Yu, B., Chen, Y. M., Wang, W., Song, Z. G., Hu, Y., Tao, Z. W., Tian, J. H., Pei, Y. Y., Yuan, M. L., Zhang, Y. L., Dai, F. H., Liu, Y., Wang, Q. M., Zheng, J. J., Xu, L., Holmes, E. C., & Zhang, Y. Z. (2020). A new coronavirus associated with human respiratory disease in China. *Nature*, *579*(7798), 265–269. https://doi.org/10.1038/s41586-020-2008-3

Xia, S., Yan, L., Xu, W., Agrawal, A. S., Algaissi, A., Tseng, C. T. K., Wang, Q., Du, L., Tan, W., Wilson, I. A., Jiang, S., Yang, B., & Lu, L. (2019). A pan-coronavirus fusion inhibitor targeting the HR1 domain of human coronavirus spike. *Science Advances*, *5*(4). https://doi.org/10.1126/sciadv.aav4580

Xiao, K., Zhai, J., Feng, Y., Zhou, N., Zhang, X., Zou, J. J., Li, N., Guo, Y., Li, X., Shen, X., Zhang, Z., Shu, F., Huang, W., Li, Y., Zhang, Z., Chen, R. A., Wu, Y. J., Peng, S. M., Huang, M., … Shen, Y. (2021). Author Correction: Isolation of SARS-CoV-2-related coronavirus from Malayan pangolins (Nature, (2020), 583, 7815, (286-289), 10.1038/s41586-020-2313-x). *Nature*, *600*(7887), E8–E10. https://doi.org/10.1038/s41586-021-03838-z

Xu, R. H., He, J. F., Evans, M. R., Peng, G. W., Field, H. E., Yu, D. W., Lee, C. K., Luo, H. M., Lin, W. S., Lin, P., Li, L. H., Liang, W. J., Lin, J. Y., & Schnur, A. (2004a). Epidemiologic clues to SARS origin in China. *Emerging Infectious Diseases*, *10*(6), 1030–1037. https://doi.org/10.3201/eid1006.030852

Xu, R. H., He, J. F., Evans, M. R., Peng, G. W., Field, H. E., Yu, D. W., Lee, C. K., Luo, H. M., Lin, W. S., Lin, P., Li, L. H., Liang, W. J., Lin, J. Y., & Schnur, A. (2004b). Epidemiologic clues to SARS origin in China. *Emerging Infectious Diseases*, *10*(6), 1030–1037. https://doi.org/10.3201/eid1006.030852

Yao, H., Song, Y., Chen, Y., Wu, N., Xu, J., Sun, C., Zhang, J., Weng, T., Zhang, Z., Wu, Z., Cheng, L., Shi, D., Lu, X., Lei, J., Crispin, M., Shi, Y., Li, L., & Li, S. (2020).

Molecular Architecture of the SARS-CoV-2 Virus. *Cell*, *183*(3), 730-738.e13. https://doi.org/10.1016/j.cell.2020.09.018

Ye, Z. W., Yuan, S., Yuen, K. S., Fung, S. Y., Chan, C. P., & Jin, D. Y. (2020). Zoonotic origins of human coronaviruses. *International Journal of Biological Sciences*, *16*(10), 1686–1697. https://doi.org/10.7150/ijbs.45472

Yu, E. D., Narowski, T. M., Wang, E., Garrigan, E., Mateus, J., Frazier, A., Weiskopf, D., Grifoni, A., Premkumar, L., da Silva Antunes, R., & Sette, A. (2022). Immunological memory to Common Cold Coronaviruses assessed longitudinally over a three-year period pre-COVID19 pandemic. *Cell Host & Microbe*. https://doi.org/10.1016/J.CHOM.2022.07.012

Yurkovetskiy, L., Wang, X., Pascal, K. E., Tomkins-Tinch, C., Nyalile, T. P., Wang, Y., Baum, A., Diehl, W. E., Dauphin, A., Carbone, C., Veinotte, K., Egri, S. B., Schaffner, S. F., Lemieux, J. E., Munro, J. B., Rafique, A., Barve, A., Sabeti, P. C., Kyratsous, C. A., … Luban, J. (2020). Structural and Functional Analysis of the D614G SARS-CoV-2 Spike Protein Variant. *Cell*, *183*(3), 739-751.e8. https://doi.org/10.1016/j.cell.2020.09.032

Zaki, A. M., van Boheemen, S., Bestebroer, T. M., Osterhaus, A. D. M. E., & Fouchier, R. A. M. (2012). Isolation of a Novel Coronavirus from a Man with Pneumonia in Saudi Arabia. *New England Journal of Medicine*, *367*(19), 1814–1820. https://doi.org/10.1056/NEJMOA1211721/SUPPL_FILE/NEJMOA1211721_DISCLOSURES.PDF

Zech, F., Schniertshauer, D., Jung, C., Herrmann, A., Cordsmeier, A., Xie, Q., Nchioua, R., Prelli Bozzo, C., Volcic, M., Koepke, L., Müller, J. A., Krüger, J., Heller, S., Stenger, S., Hoffmann, M., Pöhlmann, S., Kleger, A., Jacob, T., Conzelmann, K. K., … Kirchhoff, F. (2021). Spike residue 403 affects binding of coronavirus spikes to human ACE2. *Nature Communications 2021 12:1*, *12*(1), 1–10. https://doi.org/10.1038/s41467-021-27180-0

Zhang, A. R., Shi, W. Q., Liu, K., Li, X. Lou, Liu, M. J., Zhang, W. H., Zhao, G. P., Chen, J. J., Zhang, X. A., Miao, D., Ma, W., Liu, W., Yang, Y., & Fang, L. Q. (2021). Epidemiology and evolution of Middle East respiratory syndrome coronavirus, 2012–2020. *Infectious Diseases of Poverty*, *10*(1), 66. https://doi.org/10.1186/s40249-021-00853-0

Zhang, L., Jackson, C. B., Mou, H., Ojha, A., Peng, H., Quinlan, B. D., Rangarajan, E. S., Pan, A., Vanderheiden, A., Suthar, M. S., Li, W., Izard, T., Rader, C., Farzan, M., & Choe, H. (2020). SARS-CoV-2 spike-protein D614G mutation increases virion spike density and infectivity. *Nature Communications*, *11*(1), 6013. https://doi.org/10.1038/s41467-020-19808-4

Zhang, L., Jackson, C., Mou, H., Ojha, A., Rangarajan, E., Izard, T., Farzan, M., & Choe, H. (2020). The D614G mutation in the SARS-CoV-2 spike protein reduces S1 shedding and increases infectivity. *BioRxiv : The Preprint Server for Biology*. https://doi.org/10.1101/2020.06.12.148726

Zhao, M. M., Yang, W. L., Yang, F. Y., Zhang, L., Huang, W. J., Hou, W., Fan, C. F., Jin, R. H., Feng, Y. M., Wang, Y. C., & Yang, J. K. (2021). Cathepsin L plays a key role in SARS-CoV-2 infection in humans and humanized mice and is a promising target for new drug development. *Signal Transduction and Targeted Therapy*, *6*(1), 1–12.

https://doi.org/10.1038/s41392-021-00558-8

Zhou, H., Ji, J., Chen, X., Bi, Y., Li, J., Wang, Q., Hu, T., Song, H., Zhao, R., Chen, Y., Cui, M., Zhang, Y., Hughes, A. C., Holmes, E. C., & Shi, W. (2021). Identification of novel bat coronaviruses sheds light on the evolutionary origins of SARS-CoV-2 and related viruses. *Cell*, *184*(17), 4380-4391.e14. https://doi.org/10.1016/j.cell.2021.06.008

Zhou, P., Yang, X. Lou, Wang, X. G., Hu, B., Zhang, L., Zhang, W., Si, H. R., Zhu, Y., Li, B., Huang, C. L., Chen, H. D., Chen, J., Luo, Y., Guo, H., Jiang, R. Di, Liu, M. Q., Chen, Y., Shen, X. R., Wang, X., … Shi, Z. L. (2020a). A pneumonia outbreak associated with a new coronavirus of probable bat origin. *Nature*, *579*(7798), 270–273. https://doi.org/10.1038/s41586-020-2012-7

Zhou, P., Yang, X. Lou, Wang, X. G., Hu, B., Zhang, L., Zhang, W., Si, H. R., Zhu, Y., Li, B., Huang, C. L., Chen, H. D., Chen, J., Luo, Y., Guo, H., Jiang, R. Di, Liu, M. Q., Chen, Y., Shen, X. R., Wang, X., … Shi, Z. L. (2020b). Erratum: Addendum: A pneumonia outbreak associated with a new coronavirus of probable bat origin (Nature (1988) 81 11 (18-19)). *Nature*, *588*(7836), E6. https://doi.org/10.1038/s41586-020-2951-z

Zhu, C., He, G., Yin, Q., Zeng, L., Ye, X., Shi, Y., & Xu, W. (2021). Molecular biology of the SARs-CoV-2 spike protein: A review of current knowledge. *Journal of Medical Virology*, *93*(10), 5729–5741. https://doi.org/10.1002/jmv.27132

6. Appendix

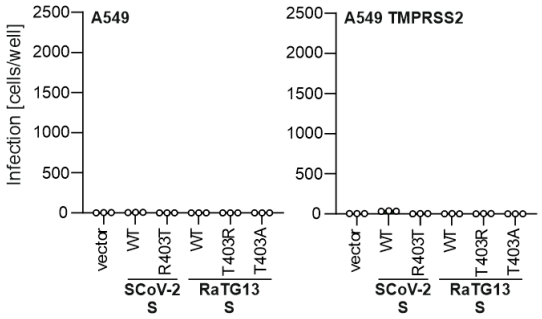

Supplementary Figure 1. A549 and A549 TMPRSS2 are not permissive for SARS-CoV-2 or RaTG13 S mediated infection. Automatic quantification of infection events of A549 and A549 TMPRSS2 expressing cells transduced with VSVΔG-GFP pseudotyped with SARS-CoV-2, RaTG13 or indicated mutant S. Bars represent the mean of three independent experiments (±SEM). Related to Fig. 2. From Zech et al., 2021 CC BY 4.0

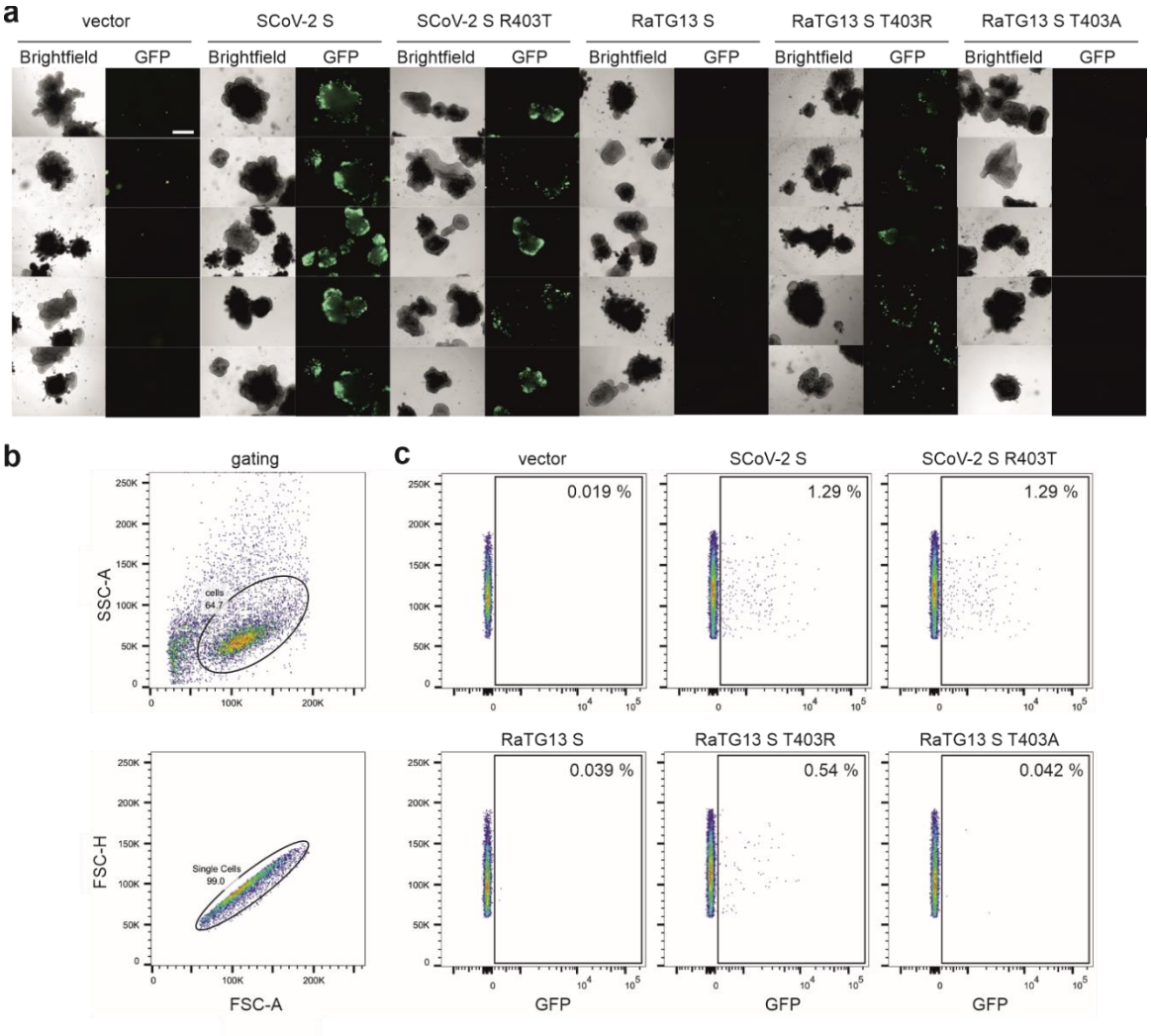

Supplementary Figure 2. T403R allows RaTG13 S to mediate infection of human intestinal organoids. a, Bright field and fluorescence microscopy (GFP) images of hPSC derived gut organoids infected with equal amounts of VSVΔG-GFP (green) pseudotyped with SARS-CoV-2, RaTG13 or indicated mutant S (2 h). Scale bar, 250µm. Related to Fig. 2. b, Exemplary gating strategy of flow cytometry-based analysis of GFP-positive cells shown in panel a. From Zech et al., 2021 CC BY 4.0

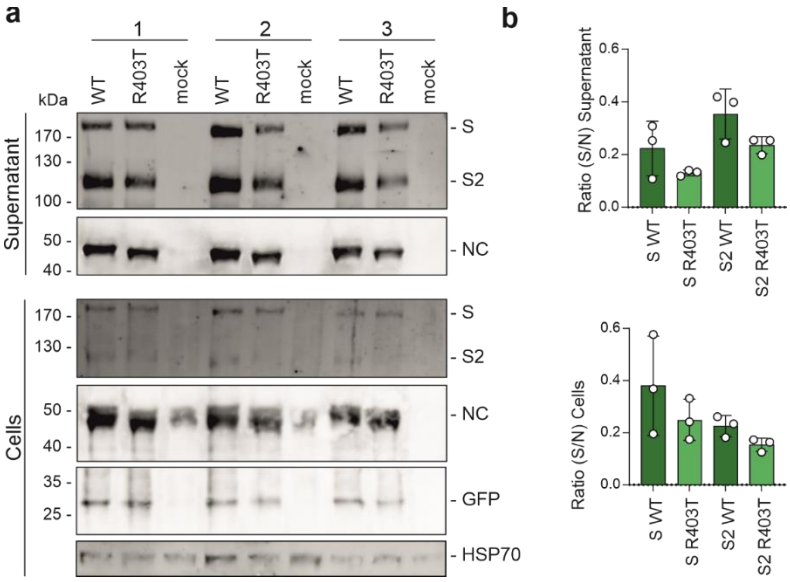

Supplementary Figure 3. Expression of WT and R403T S proteins by replication-competent SARS-CoV-2. Immunoblot of whole cells lysates (WCLs) and Supernatants of CaCo-2 cells infected with SARS-CoV-2 d6-YFP wild type or SARS-CoV-2 d6-YFP R403T. Blots were stained with anti-S, anti-N, anti-GFP and anti-HSP70 and quantified for spike expression. n=3 (biological replicates). **b,** quantification of spike in the supernatant of SARS-CoV-2 d6-YFP wild type or SARS-CoV-2 d6-YFP R403T infected CaCo-2 cells. Bars represent the mean of three independent experiments (±SEM). From Zech et al., 2021 CC BY 4.0

7. Aknowledgements

This dissertation is the result of a research project that would not have been possible without the cooperation and support of many people.

Foremost, I want to thank Frank Kirchhoff for mentoring and supporting me through my time as a graduating scientist. Your institute is an amazing place to learn, discuss and to contribute.

Thanks to Dr. Simone Joas for being awesome! … and for supervising me during the first year of my thesis. Thanks to Dr. Konstantin Sparrer for all the help, discussions and the possibility to work with so many different viruses.

Thanks to my thesis advisory committee, Prof. Dr. Timo Jacob and Prof. Dr. Florian Klein for their support and time throughout the graduation process.

Thanks to all of the collaborators who contributed to this study.

Thanks to all past and present colleagues and friends from the institute. You are the best! Thank you for the great atmosphere, the good times and all the evenings we had. You all made/make the time here, without a doubt, the most enjoyable time of my life. Furthermore, I want to thank all members of the CRC1279. It is a fantastic experience to be part of such an incredible network.

Thanks so much to Kerstin Regensburger, Regina Burger and Martha Mayer for the technical assistance during my thesis. Special thanks also to Dré van der Merwe, the man who keeps the lab running! Thanks to Rayhane Nchioua for being the most amazing S3 lab partner one could ever imagine.

Finally, thanks to my Family: Jutta, Reiner, Alexander, Mena, Lisbeth, Franz, Dani, Andrea, Willi and Mimi, for their support and patience with me during this time.

8. Statutory declaration

I hereby declare that I wrote the present dissertation with the topic:

“Substitution of T403R allows efficient utilization of human ACE2 by Spike proteins of bat coronaviruses”

independently and used no other aids than those cited. In each individual case, I have clearly identified the source of the passages that are taken word for word or paraphrased from other works.
I also hereby declare that I have carried out my scientific work according to the principles of good scientific practice in accordance with the current „Satzung der Universität Ulm zur Sicherung guter wissenschaftlicher Praxis“ [Rules of the University of Ulm for Assuring Good Scientific Practice].

Ulm,

Fabian Zech

Last Name: Zech
First Name: Fabian

Post-Doc

Since 01/2023

Institute of Molecular Virology, Ulm University Medical Center, Postdoctoral fellow in the lab of Prof. Frank Kirchhoff.

Additional Experience

Establishment of methods (infection assays, glycoprotein-receptor interaction, drug discovery and development, work under BSL 2, S3** and S3 conditions). Associated with the CRC1279, project A05 and web administration. Supervision of practical, Bachelor's and Master's students, presentation of scientific results at conferences.

Awards

Best Season Paper Award "Spring 2022" of the junge GFV

Education

06/18 – 01/23
Ulm University: PhD student at the Institute of Molecular Virology, Ulm University Medical Center, PhD thesis: "Substitution of T403R allows efficient utilization of human ACE2 by Spike proteins of bat coronaviruses"

03/15 – 06/18
Ulm University: Biochemistry M.Sc., Master thesis: "Candidate restriction factors suppress infectivity of HIV-1 particles pseudotyped with various heterologous envelope glycoproteins"

09/14 – 03/15
Bayreuth University: Student assistant, Institute for Plant Physiology

10/11 – 03/15
Bayreuth University: Biochemistry B.Sc. multiple times student assistant and supervision of practical courses. Bachelor thesis: "Functional characterization of the transcriptional factor LBD41 in *A. thaliana*."

International Experience

07/16 – 01/17
Stavanger University Norway: Biochemie M.Sc, focus on: protein chemistry

Additional Qualifications

Training: Good scientific practice (workshop)
Drug design and biochemistry (summer school)

Publications

Pastorio C[#], Zech F[#], Noettger S, Jung C, Jacob T, Sanderson T, Sparrer KMJ, Kirchhoff F. **Determinants of Spike infectivity, processing, and neutralization in SARS-CoV-2 Omicron subvariants BA.1 and BA.2. Cell Host Microbe.** doi: 10.1016/j.chom.2022.07.006., Cell Host Microbe; 2022, (# authors contributed equally)

Lawrenz J, Xie Q, Zech F, Weil T, Seidel A, Krnavek D, van der Hoek L, Münch J, Müller JA, Kirchhoff F. **Severe Acute Respiratory Syndrome Coronavirus 2 Vaccination boosts Neutralizing Activity against Seasonal Human Coronaviruses.** doi: 10.1093/cid/ciac057., Clin Infect Dis.; 2022

Nchioua R, Schundner A, Kmiec D, Prelli Bozzo C, Zech F, Koepke L, Graf A, Krebs S, Blum H, Frick M, Sparrer KMJ, Kirchhoff F. **SARS-CoV-2 Variants of Concern Hijack IFITM2 for Efficient Replication in Human Lung Cells.** doi: 10.1128/jvi.00594-22. J Virol.; 2022

Schmidt H, Gutjahr L, Sauter A, Zech F, Nchioua R, Stenger S, Frick M, Kirchhoff F, Dietl P, Wittekindt OH. **Serially passaged, conditionally reprogrammed nasal epithelial cells as a model to study epithelial functions and SARS-CoV-2 infection.** doi: 10.1152/ajpcell.00363.2021., Am J Physiol Cell Physiol; 2022

Zech F, Schniertshauer D, Jung C, Herrmann A, Cordsmeier A, Xie Q, Nchioua R, Prelli Bozzo C, Volcic M, Koepke L, Müller JA, Krüger J, Heller S, Stenger S, Hoffmann M, Pöhlmann S, Kleger A, Jacob T, Conzelmann KK, Ensser A, Sparrer KMJ, Kirchhoff F. **Spike residue 403 affects binding of coronavirus spikes to human ACE2.** doi: 10.1038/s41467-021-27180-0., Nature Communications; 2021

Prelli Bozzo C, Nchioua R, Volcic M, Koepke L, Krüger J, Schütz D, Heller S, Stürzel CM, Kmiec D, Conzelmann C, Müller J, Zech F, Braun E, Groß R, Wettstein L, Weil T, Weiß J, Diofano F, Rodríguez Alfonso AA, Wiese S, Sauter D, Münch J, Goffinet C, Catanese A, Schön M, Boeckers TM, Stenger S, Sato K, Just S, Kleger A, Sparrer KMJ, Kirchhoff F. **IFITM proteins promote SARS-CoV-2 infection and are targets for virus inhibition in vitro.** doi: 10.1038/s41467-021-24817-y., Nature Communications; 2021

González-García M, Morales-Vicente F, Pico ED, Garay H, Rivera DG, Grieshober M, Raluca Olari L, Groß R, Conzelmann C, Krüger F, Zech F, Prelli Bozzo C, Müller JA, Zelikin A, Raber H, Kubiczek D, Rosenau F, Münch J, Stenger S, Spellerberg B, Franco OL, Rodriguez Alfonso AA, Ständker L, Otero-Gonzalez AJ. **Antimicrobial Activity of Cyclic-Monomeric and Dimeric Derivatives of the Snail-Derived Peptide Cm-p5 against Viral and Multidrug-Resistant Bacterial Strains.** doi: 10.1016/j.celrep.2021.109126., Epub; 2021

Hayn M, Hirschenberger M, Koepke L, Nchioua R, Straub JH, Klute S, Hunszinger V, Zech F, Prelli Bozzo C, Aftab W, Christensen MH, Conzelmann C, Müller JA, Srinivasachar Badarinarayan S, Stürzel CM, Forne I, Stenger S, Conzelmann KK, Münch J, Schmidt FI, Sauter D, Imhof A, Kirchhoff F, Sparrer KMJ. **Systematic functional analysis of SARS-CoV-2 proteins uncovers viral innate immune antagonists and remaining vulnerabilities.** doi: 10.1016/j.celrep.2021.109126.; Cell Rep. 2021

Wettstein L, Weil T, Conzelmann C, Müller JA, Groß R, Hirschenberger M, Seidel A, Klute S, Zech F, Prelli Bozzo C, Preising N, Fois G, Lochbaum R, Knaff PM, Mailänder V, Ständker L, Thal DR, Schumann C, Stenger S, Kleger A, Lochnit G, Mayer B, Ruiz-Blanco YB, Hoffmann M, Sparrer KMJ, Pöhlmann S, Sanchez-Garcia E, Kirchhoff F, Frick M, Münch J. **Alpha-1 antitrypsin inhibits TMPRSS2 protease activity and SARS-CoV-2 infection.** doi: 10.1038/s41467-021-21972-0., Nature Communications; 2021

Braun E, Hotter D, Koepke L, Zech F, Groß R, Sparrer KMJ, Müller JA, Pfaller CK, Heusinger E, Wombacher R, Sutter K, Dittmer U, Winkler M, Simmons G, Jakobsen MR, Conzelmann KK, Pöhlmann S, Münch J, Fackler OT, Kirchhoff F, Sauter D. **Guanylate-Binding Proteins 2 and 5 Exert Broad Antiviral Activity by Inhibiting Furin-Mediated Processing of Viral Envelope Proteins.** doi: 10.1016/j.celrep.2019.04.063; Cell Reports; 2019

Conferences and Presentations

Peptide Therapeutics Forum 2022 (poster), **jGFV "One Health and zoonotic viruses"** (talk), **CROI** 2022 (poster), **Annual meeting of the GFV** 2022 (poster), **CSH Retroviruses** 2021 (poster), **MPIP Mainz** 2020 (invited talk), **CRC1279 Retreats** (several talks and posters)

Ulm, January 12th, 2023